SLAC-184
UC-34d
(E/I)

A STUDY OF RARE DECAYS OF THE K_L^o *

GREGORY J. DONALDSON

STANFORD LINEAR ACCELERATOR CENTER

STANFORD UNIVERSITY

Stanford, California 94305

PREPARED FOR THE U. S. ATOMIC ENERGY

COMMISSION UNDER CONTRACT NO. AT(04-3)-515

Manuscript Completed December 1974

Printed in the United States of America. Available from National Technical Information Service, U. S. Department of Commerce, 5285 Port Royal Road, Springfield, Virginia 22151.
Price: Printed Copy $5.45; Microfiche $1.45.

*Ph. D. Dissertation.

ACKNOWLEDGMENTS

This experiment is the product of the efforts of many individuals, and I welcome this opportunity to express my gratitude for their assistance.

I am particularly appreciative of the insight and experience of Stanley Wojcicki, who anticipated the problems before they arose. His patience during the analysis was truly remarkable, for which I offer my deepest thanks.

I would like to thank Melvin Schwartz for his assistance in conducting the experiment, and for his foresight in creating a remarkable detector.

I thank John Liu, who singlehandedly generated Monte Carlo simulations for the most bizarre decays imaginable.

I also thank Jasper Kirkby for his excellent work on the shower finding routines, as well as prolific computations during the $\pi\pi\gamma$ analysis.

I gratefully thank David Hitlin for his guidance and assistance throughout the experiment.

I would also thank Allan Rothenberg for his assistance in preparing the experimental apparatus, and Rob Kennelly for his assistance with the 2μ data.

I further offer my thanks to Dan Porat, Len Birkwood and Dale Oimette for their support in creating and maintaining the system's electronics.

I am grateful to Roger Coombes and Cliff Rassmussen for their design and construction of the mechanical aspects of the spectrometer.

I also thank Robert Messner and Robert Piccioni for many helpful discussions pertaining to the analysis procedures, as well as Robert Pearson for his help in rewiring and timing the system.

I am also deeply grateful to Margaret Ledford for her cheerful help in typing this manuscript.

Finally, all of us gratefully acknowledge the expertise of the Accelerator Staff in providing excellent running conditions.

ABSTRACT

Using the SLAC K_L^o Spectrometer Facility, we have measured the ratio $\Gamma(K_L^o \to \pi^+\pi^-\gamma)/\Gamma(K_L^o \to \text{all})$ to be $(6.2 \pm 2.1) \times 10^{-5}$. The rate and Dalitz plot distribution of 24 ± 10 events are consistent with CP conservation in this weak-electromagnetic decay. We have also set upper limits on the processes $K_L^o \to \mu^+\mu^-\gamma$, $\mu^+\mu^-\pi^o$, $\pi^+\pi^-e^+e^-$, and $\pi^o\pi^\pm e^\mp\nu$.

TABLE OF CONTENTS

LIST OF TABLES

LIST OF FIGURES

I. INTRODUCTION AND REVIEW OF THEORY

We present herein a study of several of the rare decay modes of the neutral K meson. The phenomena involved span a wide range of weak interaction topics. In general, by studying a rare process, an experimenter hopes to isolate effects which may be masked or absent in their more common relatives. One hopes thereby to measure effects present at low levels, and possibly display a completely unexpected phenomenon, or test the predictions of a particular theory. It frequently happens that theories which have been invented to describe more gross features of K-decay have implications which will only arise in rare processes. Naturally, the measurement of a small branching ratio consistent with a theory does not prove the theory. However, if the prediction is inconsistent with the measurement, then serious doubt may be cast on the validity of the model. This then, is the program: One establishes which decay channels exist, and if possible determines their properties which may then be compared with theoretical expectations. For decay modes predicted but not observed, one may set an upper limit for the occurrence, thus impeaching those theories predicting larger rates.

To become more specific: We have here a neutral K beam, and an apparatus capable of simultaneously recording the data pertinent to a considerable variety of final states. Our primary interest will be in radiative decays, so that the apparatus has been designed to require a photon shower, which will also include the many K-decays having a π^o in the final state. In principle, we are sensitive to the decays

$$K_L^o \to \pi^+\pi^-\pi^o$$

$$K_L^o \to \pi^+\pi^-\gamma$$

$$K_L^o \to \mu^+\mu^-\gamma$$

$$K_L^o \to e^+e^-\gamma$$

$$K_L^o \to \mu^+\mu^-\pi^o$$

$$K_L^o \to e^+e^-\pi^o$$

$$K_L^o \to \pi^\pm e^\mp \nu\gamma$$

$$K_L^o \to \pi^+\pi^-e^+e^-$$

$$K_L^o \to \pi^+\pi^-\pi^o\gamma$$

This is quite an assortment, and it should be clear at the outset that not only will some of these processes be very rare indeed, but that the spectrometer is relatively ill-adapted for certain of the decays mentioned above. The decay $K_L^o \to 3\pi$ occurs at a branching ratio of order 10^{-1}, and will serve as a normalization, whereas the next most likely decay is $K_L^o \to \pi e\nu\gamma$ which is expected to occur with a branching ratio of order 10^{-3}. We observe only the rare decay $K_L^o \to \pi\pi\gamma$, and are thus left with the task of setting upper limits on the others. Each of these decays is predicted to occur at one level or another, and therefore a useful criterion for whether an upper limit is interesting or not is how it compares with the expected value for the branching ratio. In many cases, we are orders of magnitude from an interesting result, and therefore correspondingly little effort has gone into refining the measurement.

The wide variety of theoretical input to calculate the above rates makes for some difficulty in organizing the discussion of each of the decays in turn. For example, the motivation for a study $K_L \to \pi\pi\gamma$ and $\mu\mu\gamma$ is to some extent historical, in that a good deal of theoretical effort was expended concerning the relationship of these decays to $K_L \to \mu\mu$. The calculations predicting their

relative rates do not overlap however, and in this regard it is perhaps best to discuss $K_L \to \pi\pi\gamma$ alone. The decays $K_L \to \ell\bar{\ell}\gamma$ (where ℓ indicates e^- or μ^-) occur naturally together, either arising from the Dalitz pair process $K_L^o \to \gamma\gamma$ followed by $\gamma \to \ell\bar{\ell}$, or from a direct process possibly involving neutral currents. The decays $K_L^o \to \ell\bar{\ell}\pi^o$ are discussed concurrently, since they share the neutral current aspect of $\ell\bar{\ell}\gamma$. The decays $K_L^o \to \pi e\nu\gamma$ and $\pi\pi\pi^o\gamma$ occur primarily in this experiment as bremsstrahlung from common K_{e3}^o and $K_{\pi 3}^o$ decays, however if one could isolate possible direct emission terms something of the electromagnetic structure of the kaon would be revealed. In the case of $K_{e3\gamma}$, this process could occur at the $10^{-4} - 10^{-5}$ level,[1,2] however, for the $K_{\pi 3\gamma}$, the rate would be $\sim 10^{-7}$.[3] The former occurs as a background process and is discussed, the latter is negligibly small.

The decay $K_L^o \to \pi\pi\gamma$ offers several points of theoretical interest: The opportunity to observe another instance of CP noninvariance, a potential testing ground for theoretical models of weak radiative decays, and the possibility that this decay could interfere destructively as an intermediate state in the process $K_L^o \to \mu\mu$.

A. CP Violation and the Decay $K_L^o \to \pi^+\pi^-\gamma$

It has been pointed out some time ago that there is relatively little evidence that the electromagnetic interactions of strongly interacting particles are invariant under C and T.[4] If one suspects that the apparent CP violation has its origin in the electromagnetic interaction, then one would presumably first look at a radiative decay in the K system, since to date this is the only system in which CP invariance is violated. The decays of this type with the highest branching ratio are the $K \to \pi\pi\gamma$ decays, and for this reason several experiments have used these decays to search for CP-violating effects. In

the system of K mesons, various possibilities can exist for $K \to \pi\pi\gamma$:

$$K^+ \to \pi^+\pi^o\gamma$$

$$K^- \to \pi^-\pi^o\gamma$$

$$K_L^o \to \pi^+\pi^-\gamma$$

$$K_S^o \to \pi^+\pi^-\gamma$$

All of these decays can proceed through "inner bremsstrahlung" (IB) wherein the photon is radiated from one of the charged pions in $K_{\pi 2}$ decay. Secondly, it is possible, if the $K \to 2\pi$ decay proceeds through virtual intermediate states, that the photon may be emitted from one of the intermediate charged particles. This process is termed "direct emission", (DE) and is much less straightforward to calculate due to the large number of possible intermediate states. In general, the rates for the direct processes depend on the specific constituents in the model for the decay, and are not necessarily related in any simple way. Experimental searches have been carried out for all of the above decays, and it is only recently that observation of any direct process has been reported.

In the decay $K^\pm \to \pi^\pm\pi^o\gamma$, direct emission can proceed at a rate comparable to inner bremsstrahlung since the direct process involves no violation of the $\Delta I = 1/2$ rule, and the decay $K_{\pi 2}$ is highly surpressed. For this reason, the $K^\pm$ decay was considered an excellent experimental prospect, and in 1972 the first evidence for the direct terms was published.[5] The observation favored pure magnetic dipole emission, since there were no CP violating asymmetries[6] between K^+ and K^- decay which would arise from electric dipole emission.

Inner bremsstrahlung strongly dominates the decay $K_S \to \pi^+\pi^-\gamma$, since the $K_S^o \to \pi^+\pi^-$ is the preferred decay mode. Although surpressed, direct emission

is still possible, and would likely proceed via electric-dipole emission (E1), since the K_S is an approximate CP (+) eigenstate. To date, no experimental evidence has been published to confirm the existence of direct emission in the K_S system, however the present limits are rather insensitive. In 1973, Burgen et al.[7] reported a measurement of $K_S^o \to \pi\pi\gamma$, wherein they see only a bremsstrahlung distribution. If they take the difference between their measurement and the theoretical rate for bremsstrahlung, they are able to set a quasi-upper limit $\Gamma(K_S^o \to \pi\pi\gamma, \text{ direct})/\Gamma(K_S^o \to \pi\pi) \leq (0.3 \pm 0.6) \times 10^{-3}$ which implies that $\Gamma(K_S^o \to \pi\pi\gamma, \text{ direct})/\Gamma(K_S^o \to \text{all}) \leq (.2 \pm .4) \times 10^{-3}$, using $\Gamma(K_S^o \to \pi\pi)/\Gamma(K_S^o \to \text{all}) = 68.81\%$.

In the decay $K_L^o \to \pi\pi\gamma$, CP nonconservation may be observed in several ways.[8] First, there is a possible charge asymmetry in the momentum of the π^+ and π^- [9] which would arise from the interference of p and d waves of the $\pi\pi$ system. However even if CP violation were large in the matrix element, the expected result can attain a maximum of a few percent since the $\pi\pi$ scattering phase shifts in the p and d waves are quite small. We observe only about 25 $\pi\pi\gamma$ events and are able to make no claims for any such asymmetry. Second, there is the possibility of observing interference between the decays $K_{L,S} \to \pi\pi\gamma$.[10,11] Since only identical states can interfere, an interference would imply that the K_L and K_S are not pure CP eigenstates, which is of course already known from other experiments. Finally, both the expected rate and the energy distribution of the photon is sensitive to the CP nature of the final state.[12]

To consider the CP of the final state, it is convenient to make a simple angular momentum decomposition for which the quantum numbers are shown in Table 1. The $\pi\pi$ state is likely to have L=0, 1 or 2 since the available

Table 1

Quantum Numbers of the Final State for $K_L^o \to \pi^+\pi^-\gamma$

	M1	E1	M2	E2
$\ell_{\pi^+\pi^-}$	1	1	2	2
j_γ	1	1	2	2
$I_{\pi\pi}$	1	1	0,2	0,2
$C_{\pi\pi\gamma}$	1	1	-1	-1
$P_{\pi\pi\gamma}$	-1	+1	-1	+1
$CP_{\pi\pi\gamma}$	-1	+1	+1	-1

$$C_{\pi\pi\gamma} = (-1)^{\ell_{\pi^+\pi^-}} (-1)_{\text{photon}}$$

$$P_{\pi\pi\gamma} = \begin{cases} (-1)^{\ell_{\pi\pi}} (-1)^{j_\gamma + 1} & \text{magnetic multipoles} \\ (-1)^{\ell_{\pi\pi}} (-1)^{j_\gamma} & \text{electric multipoles} \end{cases}$$

energy of 215 MeV makes higher L extremely unlikely. No transition can occur with L=0 due to gauge invariance. (No $0 \to 0$ transition is a familiar rule for gamma emission.) Both the data from K_S decays and $K^\pm$ decays favor the lowest multipole emission, therefore let us consider the energy distribution for $L_{\pi\pi} = 1$, CP (+ and -) states from the K_L. Inner bremsstrahlung (E1, CP^+) has a characteristic divergence at low gamma momentum, whereas direct emission (M1, CP^-) tends to peak at $p_\gamma \approx 140$ MeV. In addition, the ratio $\Gamma(K_L^o \to \pi^+\pi^-\gamma, \text{ IB})/\Gamma(K_L^o \to \pi^+\pi^-) = (1.1) \times 10^{-2}$ for $E_\gamma > 10$ MeV and 0.26×10^{-2} for $E_\gamma > 50$ MeV, corresponding to a total branching ratio $(1.95) \times 10^{-5}$ and

$(.47) \times 10^{-5}$ respectively.[13] Thus we will compare both our measured rate and the energy distribution with the prediction for CP-violating inner bremstrahlung.

B. Calculations of the Decay Rate $\Gamma(K_L^o \rightarrow \pi^+\pi^-\gamma)$

Theoretical efforts to calculate the rate for $K_L \rightarrow \pi\pi\gamma$ have existed over the past decade.[14,15,16,17] The earlier models primarily employed boson poles with various assumptions necessary to establish coupling constants. These are well described by R. C. Thatcher[18] and are summarized in Table 2. In 1967, Lai and Young[13] used the method of current algebra and the PCAC hypothesis to calculate the ratio $\Gamma(K_L^o \rightarrow \pi^+\pi^-\gamma,\ M1)/\Gamma(K_L^o \rightarrow \gamma\gamma) = 0.14$. The present branching ratio[19] for $K_L \rightarrow \gamma\gamma = 4.9 \times 10^{-4}$ implies $\Gamma(\pi\pi\gamma)/\Gamma(\text{all}) = 6.86 \times 10^{-5}$ which is consistent with our result. Since that time, there have been several more attempts, including another pion pole model by R. Rockmore in 1970,[20] and a model involving a hypothetical abnormal vector meson invented by S. Barshay in 1971.[21] Neither of these gives a rate consistent with the measured branching ratio. More recently, two models for weak radiative decays have gained prominence.

M. Moshe and P. Singer consider the possibility of a description of several weak radiative decays of K mesons, based on a phenomenological Lagrangian model which is fit to data from strong and radiative decays.[22] Their model has been applied to several K decays: $K_L^o \rightarrow \gamma\gamma$, $K^+ \rightarrow e^+\nu\gamma$, $K^+ \rightarrow \pi^+\pi^o\gamma$, $K^+ \rightarrow \pi^+\gamma\gamma$ and $K_L^o \rightarrow \pi^+\pi^-\gamma$. Within this framework, they were able to obtain reasonable agreement with the $K_L^o \rightarrow 2\gamma$ experimental result,[23] having used the decay $K^+ \rightarrow e^+\nu\gamma$ to set a constraint on one of the parameters of the model. They are then able to predict[24] that the magnetic dipole transition will predominate over the electric dipole transition for $K^+ \rightarrow \pi^+\pi^o\gamma$. Using the experimentally measured rate for the magnetic transition in this decay gives a further

constraint and allows them to predict $\Gamma(K^+ \rightarrow \pi^+\gamma\gamma)/\Gamma(K^+ \rightarrow \text{all}) = (2.4 \pm 1.2) \times 10^{-6}$ and $\Gamma(K_2^o \rightarrow \pi^+\pi^-\gamma)/K(K^o \rightarrow \text{all}) = \left(4.7^{+\ 0.5}_{-\ 0.2}\right) \times 10^{-4}$. As we shall see, this rate is roughly an order of magnitude above the measured value. This model involves certain SU_3 symmetry breaking parameters mentioned above, and described in detail by P. Singer.[25] Unfortunately for this approach, a certain combination of these parameters depends on the decay rate for $\eta \rightarrow 2\gamma$. A new measurement[26] of $\Gamma(\eta \rightarrow \gamma\gamma)$ implies that the M-S model no longer gives satisfactory agreement with the experimental value for $\Gamma(K_L^o \rightarrow \gamma\gamma)$ which is fundamental to their calculation of $\Gamma(K_L^o \rightarrow \pi\pi\gamma)$. These developments are rather recent, and it remains to be seen whether they can be incorporated into the model in a consistent manner.

The other recent approach to the radiative decays of K mesons is an extension of Steinberger's baryon loop model[27] originally proposed to calculate the π^o lifetime. Rockmore and Wong[28] applied this technique to a calculation of $K_L^o \rightarrow \gamma\gamma$ and obtained $\Gamma(K_L^o \rightarrow \gamma\gamma)/\Gamma(K_L^o \rightarrow \text{all}) = 1.35 \times 10^{-4}$ to be compared with the experimental value 4.9×10^{-4}. This agreement was quite surprising considering that the calculation involves no free parameters, and that the agreement is no worse than in the case of the π^o. They then proceeded to calculate the rate $\Gamma(K^+ \rightarrow \pi^+\pi^o\gamma)$,[29] for which the experimental result[5] is $\Gamma(K^\pm \rightarrow \pi^\pm\pi^o\gamma, M1)/\Gamma(K^\pm \rightarrow \text{all}) = (1.56 \pm 0.35) \times 10^{-5}$ for the kinematic range $55\ \text{MeV} < T_{\pi^\pm} < 90\ \text{MeV}$. For the same region of phase space, their theoretical result is uncannily accurate: $\Gamma(K^\pm \rightarrow \pi^\pm\pi^o\gamma, M1)/\Gamma(K^+ \rightarrow \text{all}) = (1.56) \times 10^{-5}$. Using the same model Rockmore and Kamal[30] calculate the decay $K^+ \rightarrow \pi^+\gamma\gamma$ a branching ratio $\Gamma(K^+ \rightarrow \pi^+\gamma\gamma)/\Gamma(K^+ \rightarrow \text{all}) = 0.64 \times 10^{-6}$, for which the present upper limit is $BR < 3.5 \times 10^{-5}$.

Table 2

Calculations for $R = \Gamma(K_L^o \to \pi^+\pi^-\gamma)/\Gamma(K_L^o \to \text{all})$

Theorist	Date		Result
Chew	1962	Boson pole approximation	No quantitative result
Pepper and Ueda	1964	Boson pole approximation	6.7×10^{-4}
Oneda, Kim and Korff	1964	Boson pole approximation	2.9×10^{-5}
Cline	1965	$\Delta I = \frac{1}{2}$ rule	$\leq 2 \times 10^{-3}$
Lai and Young	1967	Current Algebra, PCAC	$(6.8 \pm 0.6) \times 10^{-5}$
		Inner bremsstrahlung	1.95×10^{-5}; $E_\gamma > 10$ MeV
			0.47×10^{-5}; $E_\gamma > 50$ MeV
Rockmore	1970	Pion pole model, Veneziano model	$9.14 \times 10^{-5} < R < 3.1 \times 10^{-4}$
Barshay	1971	Hypothetical $\tilde{\rho}_0$ meson	1.04×10^{-5}
Moshe and Singer	1972	Phenomenological Lagrangian, SU(3) breaking	$2.6 < R < 4 \times 10^{-4}$
Moshe and Singer	1973	Details of constants adjusted	$\left(4.7 \begin{smallmatrix} +0.5 \\ -0.2 \end{smallmatrix}\right) \times 10^{-4}$
Rockmore and Wong	1973	Modified fermion loop model	7.8×10^{-5}
Experimental Results			
Anikina et al.	1966	Cloud chamber	< 0.02
Bellotti et al.	1966	Heavy liquid bubble chamber	$< 5 \times 10^{-3}$
Nefkens et al.	1966	Spark chambers	$< 3 \times 10^{-3}$
Thatcher et al.	1968	Spark chambers	$< 4 \times 10^{-4}$
This experiment	1973	Wire spark chambers	$(6.2 \pm 1.9) \times 10^{-5}$

In the case of the decay $K_L^o \to \pi\pi\gamma$, the calculation[31] yields directly the value $\Gamma(K_L^o \to \pi^+\pi^-\gamma)/\Gamma(K_L^o \to \text{all}) = 7.5 \times 10^{-5}$. Prior to the publication[32] of the experimental $\pi\pi\gamma$ branching ratio (which is consistent with this zero free parameter result), Rockmore and Wong had argued that it would be more reliable to renormalize the $\pi\pi\gamma$ branching ratio by the factor $\Gamma(K_L^o \to \gamma\gamma, \text{experimental})/\Gamma(K_L^o \to \gamma\gamma, \text{theoretical})$ to account for the discrepancy between their theory and the experimental value for $K_L^o \to \gamma\gamma$. In light of the consistency with the unrenormalized result this appears to be unnecessary, and for the moment the $K_L^o \to \gamma\gamma$ discrepancy will remain unexplained. In view of the widespread agreements between this model and experimental results, it seems that this calculational technique for radiative decays has considerable predictive power.

C. <u>The Decay $K_L^o \to \pi^+\pi^-\gamma$ and the $K_L^o \to \mu^+\mu^-$ Puzzle</u>

Historically, the controversy over an experimental result for $K_L^o \to \mu^+\mu^-$ spurred a great deal of activity, not only to search for weak neutral currents, but to understand why this decay appeared to contradict a fundamental lower limit for its rate. To review the situation,[33,34] in 1971 a Berkeley group reported $\Gamma(K_L^o \to \mu^+\mu^-)/\Gamma(K_L^o \to \text{all}) \leq 1.8 \times 10^{-9}$ at 90% C.L.[35] On the other hand, it is possible on very general grounds to calculate a "primitive unitarity limit" which is $\Gamma(K_L^o \to \mu^+\mu^-)/\Gamma(K_L^o \to \text{all}) > 5 \times 10^{-9}$.[36] The minimal assumptions involved are CPT and CP invariance and unitarity. Essentially the idea is that if the K_L can decay to $\gamma\gamma$, then the $\gamma\gamma \to \mu\mu$ rate can be calculated using QED. One finds that $\Gamma(K_L^o \to \mu\mu)/\Gamma(K_L^o \to \gamma\gamma) \geq 0.96 \times 10^{-5}$ which yields the limit quoted above.

Now it may happen that the decay $K_L^o \to \pi\pi\gamma$ may interfere with the $\mu\mu$ amplitude via the process shown in Fig. 1.

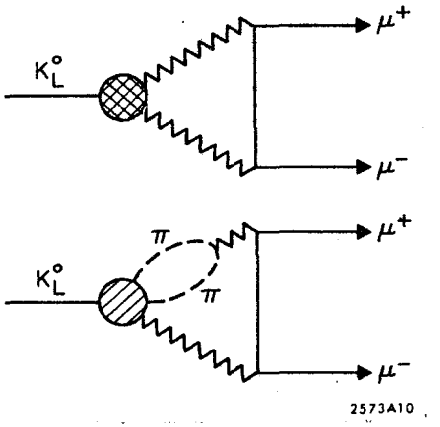

FIG. 1--Processes contributing to $K_L^o \to \mu\mu$.

The estimate for the absorption utilized the previous upper limit for the $\pi\pi\gamma$ rate, so that a lower experimental value is guaranteed to reduce the effect further. Previous experimental work[37,38,39,40] had established $R = \Gamma(K_L^o \to \pi^+\pi^-\gamma)/\Gamma(K_L^o \to \text{all}) < 4 \times 10^{-4}$. It was originally proposed that the suppression to the $K_L^o \to \mu\mu$ rate could reach 20%,[41] however subsequent recalculations[42] reduced this estimate to ~4%. The most detailed of these is by Alles, Gaillard and Pati[43] who find that the suppression depends on a factor $\left\{\Gamma(K_L^o \to \pi\pi\gamma)/\Gamma(K_L^o \to \gamma\gamma)\right\}^{1/2}$, and that possible reductions due to other intermediate states are negligible.

Experimentally, the situation appears to have resolved itself with the discovery of 12 $K_L^o \to \mu\mu$ events at a spectrometer at Brookhaven National Laboratory. These events were found in two experiments[44,45] giving branching ratios $\Gamma(K_L^o \to \mu^+\mu^-)/\Gamma(K_L^o \to \text{all}) = \left(11^{+10}_{-5}\right) \times 10^{-9}$ and $\left(14^{+13}_{-7}\right) \times 10^{-9}$ respectively. It should be noted that in both cases, the normalization

is to the decay $K_L \to \pi^+\pi^-$, and that these results depend on $|\eta_{+-}|$. Taking $|\eta_{+-}| = (2.29 \pm 0.026) \times 10^{-3}$, the experiments can be combined to give an average $\left(12^{+8}_{-4}\right) \times 10^{-9}$. Furthermore, the Berkeley group is reanalyzing their data and has quoted[46] $\Gamma(K_L^o \to \mu^+\mu^-)/\Gamma(K_L^o \to \text{all}) < 3.4 \times 10^{-9}$.

D. The Decays $K_L^o \to \ell\bar{\ell}\gamma$ and $\ell\bar{\ell}\pi^o$

Weak decays in which two leptons with zero total charge occur in the final state have long been an object of theoretical interest. The original motivation lay in the possibility that there might be a direct coupling (possibly via a neutral intermediate vector boson) of a weak neutral lepton current to the weak hadron current postulated in various theories of the $\Delta I = 1/2$ rule. The experimental upper limits for such processes have steadily decreased, and it is clear that if such currents exist their coupling is much weaker than that of charged currents. There are various models which incorporate this fact in one way or another, and it remains as a challenge to the proposed gauge theories of weak interactions to reproduce the very small rates for strangeness changing neutral current processes.

An elementary discussion of the difficulties in gauge theories with $\Delta S = \pm 1$, $\Delta Q = 0$ leptonic processes was given by Joel Primack at the SLAC Summer Conference in 1973.[47] He points out that these processes are not suppressed at all in a simple hadronic extension of the Weinberg model, and a consideration of the decay $K^+ \to \pi^+e^+e^-$ yields a branching ratio nearly four orders of magnitude too large. With the Weinberg 3-quark model ruled out by K^+ decay, he then demonstrates that the Georgi-Glashow 5-quark model is in difficulty with $K_L^o \to \mu\mu$ decay. One expects a branching ratio something like 3×10^{-4}, when the experimental limit is of order 10^{-8}. One way to avoid this catastrophe is to add another symmetry, corresponding to an additional

"charmed" quark. The result is that strangeness changing amplitudes will then be proportional to $\Delta m/M_W$ where Δm is a parameter which measures the breaking of this new symmetry. Further work is progressing on these ideas, as discussed in the paper of M. K. Gaillard and Ben Lee.[48]

For the moment, we return to the decay $K_L^o \to \ell\bar{\ell}\gamma$, where the ℓ denotes either a muon or an electron.[49] In the same sense that $K_L^o \to \gamma\gamma$ guarantees the existence of $K_L^o \to \mu\mu$, we have here a process that is at least one order lower in α in the electromagnetic interaction alone without invoking a neutral current process at all. The calculation of the Dalitz pair rate $\Gamma(K_L \to \ell\bar{\ell}\gamma)/\Gamma(K_L \to \gamma\gamma)$ is relatively straightforward, and yields a ratio of 1.6×10^{-2} for electrons and 4.1×10^{-4} for muons.[50] This decay may also exhibit structure effects due to a form factor parametrized by the lepton pair mass.[51] This would modify the expected branching ratios slightly (see Table 3) and would appear as a small distortion of the lepton pair mass spectrum. It may also happen that this process does in fact proceed through some sort of neutral-current mechanism; one such possibility has been considered using a Hamiltonian proposed by Wolfenstein. The original motivation was to explain the $K_L^o \to \mu\mu$ result by allowing a destructively interfering, CP violating transition $K_S \to \mu\mu$. Using this Hamiltonian, Singh has calculated[52] a branching ratio for the decay $K_L^o \to \mu\mu\gamma$, for which he obtains 3.4×10^{-7}, which is roughly twice the Dalitz pair rate. Finally, a model proposed by Alles and Pati[53] involving an hitherto undetected light neutral boson decaying to μ-pairs would predict a very large rate for $K_L^o \to \mu\mu\gamma$, on the order of 6×10^{-4}. The sensitivity of this experiment extends to branching ratios on the order of 10^{-6}, so that we will be able to detect this decay if it exists.

A measurement of the decay $K_L^o \to \ell\bar{\ell}\pi^o$ could serve as a test of several interesting theoretical ideas. The decay could proceed as a second order weak process, or alternatively could arise as an electromagnetic effect superimposed on a lowest-order nonleptonic interaction. In other models still other couplings are present and this decay will eventually test the predictions of the recent gauge models. Not only is this a testing ground for neutral current predictions, but if sufficient data could be acquired it might become possible to determine whether or not there is a nonlocal lepton coupling.

The concept of lepton nonlocality is certainly only speculation at the present time, however it is interesting to note that Greenberg and Yodh propose[54] that a finite lepton size contributes to the lack of 1/s behavior of the cross section for $e^+e^- \to$ hadrons. Further in the realm of speculation is the possibility of observing the decay of heavy leptons via the process $K \to L\bar{\ell}$ followed by $L \to \pi\ell$. These ideas have been summarized in two papers; Pais and Treiman[55] and Singh and Wolfenstein,[56] and the assorted branching ratio predictions are given in Table 3.

Reliable calculations for higher order weak interactions are very difficult, and only one estimate for $K_L \to \ell\bar{\ell}\pi^o$ appears in the literature. This arises in the model of Okubo and Bace,[57] who consider a triplet (or octet) of intermediate vector bosons which have strong interactions among themselves but are coupled weakly (or electromagnetically) to all other particles. This model is aimed at the decay modes $K_{L,S}^o \to \mu^+\mu^-$, however, it also allows a calculation of the rates for $K_L^o \to \ell\bar{\ell}\pi^o$, $\pi^+\pi^-e^+e^-$, and $\pi^o\pi^\pm e^\mp\nu$. The model suppresses the decay $K_L^o \to \mu\mu$, however the $K_S^o \to \mu\mu$ decay must satisfy a lower bound $\Gamma(K_S^o \to \mu^+\mu^-)/\Gamma(K_S^o \to \text{all}) \geq 1.6 \times 10^{-7}$. This formulation also gives rise to a new CP violating neutral leptonic interaction and predates the gauge-theory

quark models. Their result is $K_L^o \to e^+e^-\pi^o \lesssim 1.65 \times 10^{-6}$ and $\Gamma(K_L^o \to ee\pi^o)/\Gamma(K_L^o \to \mu\mu\pi^o) \simeq 0.32$. This appears to contradict the recent result,[58] $\Gamma(K^+ \to \pi^+e^+e^-)/\Gamma(K^+ \to \text{all}) = (2.3 \pm 0.8) \times 10^{-7}$. A paper of Gaillard and Lee[48] presents several estimates for rare kaon decays, and in the context of branching ratios of order $10^{-8} - 10^{-13}$ they predict the decay $K_L^o \to e^+e^-\pi^o$ will be "strongly suppressed". Interestingly, the Gaillard and Lee prediction for $K_S^o \to \mu\mu$ is less than 10^{-13}, so that an observation of both these rates will serve to discriminate between these considerations and the Okubo and Bace model. In addition the decay $K_S^o \to \pi^o e^+e^-$ will test the baryon loop model[59] ($\Gamma(K_S^o \to \pi^o e^+e^-) \approx 0$) against the gauge-theory prediction ($\Gamma(K_S^o \to \pi^o e^+e^-) \approx 10^{-8}$).

E. The Decays $K_L^o \to \pi^+\pi^-e^+e^-$ and $\pi^o\pi^\pm e^\mp\nu$

The four-body decays of the K_L are poorly understood, both from the theoretical point of view, and as a matter of experimental difficulty. At this time, only a few four-body branching ratios are published for the neutral kaon: The Russian streamer chamber result for $K_L^o \to \pi\pi ee$ [60] and a CERN bubble chamber result for $K_L \to \pi e\nu + \gamma$.[61] Again, the predictions and the experimental values are displayed in Table 3.

Experimentally, the decay $K_L \to \pi\pi ee$ will be highly constrained, since the probability of verticizing accidental tracks into a four-pronged decay is very low so that the background will be suppressed. In this case, the process wherein the lepton pair originates in the photon from $K_L \to \pi\pi\gamma$ decay is very small, since the $\pi\pi\gamma$ rate itself is of order 10^{-5}. Thus the $\pi\pi ee$ decay is expected to be dominated by a pole graph[62] as shown in Fig. 2 although $K_L^o \to \pi^+\pi^-\gamma$ could contribute via a Dalitz pair mechanism. In this case, the transition is sensitive to the electromagnetic form factor of the K_L^o, which in turn could provide

Table 3

Calculations for $R = \Gamma(K_L^o \rightarrow \text{rare mode})/\Gamma(K_L^o \rightarrow \text{all})$

Decay	Theorist		Result
$K_L^o \rightarrow \ell\bar{\ell}\gamma$	Miyazaki	Dalitz pairs and $K_L \rightarrow \gamma\gamma$ rate.	8.3×10^{-6} for $ee\gamma$ 2.1×10^{-7} for $\mu\mu\gamma$
	Singh	CP odd nonelectromagnetic interactions, "Wolfenstein Hamiltonian".	$(2.2\text{-}5.2) \times 10^{-7}$ for $ee\gamma$ $(1.5\text{-}3.4) \times 10^{-7}$ for $\mu\mu\gamma$
	Alles and Pati	Light neutral boson decaying to $\mu^+\mu^-$.	$> 6 \times 10^{-4}$ for $\mu\mu\gamma$
	Sehgal	Various structure effects in matrix element.	$(7.8\text{-}8.1) \times 10^{-6}$ for $ee\gamma$ $(2.0\text{-}2.7) \times 10^{-7}$ for $\mu\mu\gamma$
		Experimental upper limit. No experimental upper limit for $\mu\mu\gamma$.	$(< 2.8 \times 10^{-7})$ for $ee\gamma$
$K_L^o \rightarrow \ell\bar{\ell}\pi$	Okubo and Bace	Strong internal coupling among intermediate vector bosons (IVB).	$\lesssim 1.65 \times 10^{-6}$ for $ee\pi$ $\lesssim 0.65 \times 10^{-6}$ for $\mu\mu\pi$
	Pais and Trieman	Order of magnitude estimate. No experimental upper limit.	$\sim 10^{-6}$
$K_L^o \rightarrow \pi^o\pi e\nu$	Weinberg	Current algebra and PCAC.	5×10^{-5}
	Okubo and Bace	IVB model.	1.23×10^{-4}
	Behrends, Okubo and Bace	Fit to $K^{\pm}$ data. No experimental upper limit.	$0.79\text{-}1.2 \times 10^{-4}$
$K_L^o \rightarrow \pi^+\pi^-e^+e^-$	Majumador and Smith	Vector meson dominance, current algebra, $K_L \rightarrow \gamma\gamma$ rate.	1.7×10^{-7}
	Bace and Okubo	IVB model.	3.4×10^{-9}
	Anikina et al.	Experimental upper limit.	$< 3.0 \times 10^{-5}$

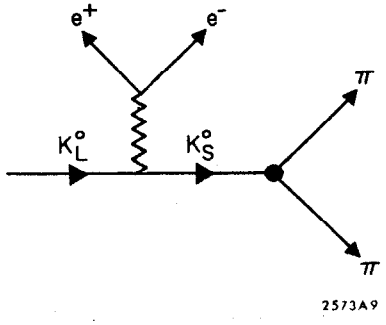

FIG. 2--Pole graph for $K_L^o \to \pi^+\pi^- e^+ e^-$ via a $K_L \to K_S \gamma$ transition.

information about the charge radius or 'size' of the kaon through the relation[63]

$$F_{K^o}(t) \approx \frac{1}{6}\, t\, R_K^2$$

where $R_K = \sqrt{\langle r^2 \rangle}$, $\langle r^2 \rangle$ = mean squared charged distribution radius, and $F_{K^o}(t)$ = electromagnetic form factor of K_L^o. Majumador and Smith[64] use a vector-meson dominance model to evaluate the mean-square radius, and a current algebra calculation for $K_L^o \to \pi\pi\gamma$ [13] to obtain $\Gamma(K_L^o \to \pi^+\pi^- e^+ e^-)/\Gamma(K_L^o \to \text{all}) = 1.7 \times 10^{-7}$. This decay rate is also predictable in the intermediate vector boson model of Okubo and Bace[57] who obtain a branching ratio $> 3.4 \times 10^{-9}$ for the direct process.

The decay $K_L \to \pi^o \pi^\pm e^\mp \nu$ is the neutral analog of the charged K_{e4} decays. One of the interesting features of this decay is its potential to differentiate among several schemes for the parametrization of K_{e4} form factors. An analysis of Pais and Trieman[65] defines a useful description of the K_{e4} matrix elements which contains information relating to the π-π phase shifts over a certain energy range. Several experiments[66,67,68] involving charged K_{e4} decays has not been able to resolve which of several choices of experimental parameters is favored by the data. Using the results from charged K decays, it is possible to compute the $K_L^o \to \pi^o \pi^\pm e^\mp \nu$ branching ratio,[69,70] and compare the disparate experimental values. Since the results are quite distinctive, the K_L^o four-body branching ratio may allow a choice among several results.

There is also a calculation by Weinberg[71] using current algebra techniques and PCAC, for which he obtains $\Gamma(K_L^o \to \pi^-\pi^o e^+\nu)/\Gamma(K^+ \to \pi^+\pi^- e^+\nu) = 0.16$. Using the published values $\Gamma(K^+ \to \pi^+\pi^- e^+\nu)/\Gamma(K^+ \to \text{all}) = 3.7 \times 10^{-5}$ and $\tau_{K_2^o} = 5.18 \times 10^{-8}$ sec and $\tau_{K^+} = 1.24 \times 10^{-8}$ sec, we have $\Gamma(K_L^o \to \pi^-\pi^o e^+\nu)/\Gamma(K_L^o \to \text{all}) = 2.48 \times 10^{-5}$. Experimentally, this decay presents considerable problems due to its kinematic similarity to $K_L \to \pi\pi\pi^o$ which will constitute a large background.

To sum up these many considerations, we have seen that the body of theoretical input spans a very wide range of weak interactions topics, and each of these decays can contribute something to the understanding of the field. Unfortunately, the rates for higher-order weak processes are extremely low, and will take a patient experimenter indeed to collect enough data to answer the questions raised above. This experiment collected and identified roughly 165,000 $K_L \to \pi^+\pi^-\pi^o$ decays, which account for about 10% of the total decays. Under the crude assumptions of constant experimental acceptance, this would imply that we would detect only 1-2 events at a branching ratio of 10^{-6}. In the immediate future, another radiative K decay experiment is underway at Brookhaven National Laboratory,[72] where the spectrometer that detected the $K_L^o \to \mu^+\mu^-$ decay has been modified with lead glass counters to study K^o radiative decays. Using our $\pi\pi\gamma$ branching ratio, they should obtain 10,000-15,000 $\pi\pi\gamma$ events, and roughly 30 $\mu\mu\gamma$ events. This should allow them to detect both the direct and inner bremsstrahlung decay of $K_L^o \to \pi^+\pi^-\gamma$, as well as establish a branching ratio for $K_L^o \to \mu^+\mu^-\gamma$.

II. THE SLAC K^O SPECTROMETER FACILITY

The experiment was conducted at the SLAC K^O Spectrometer Facility, where we observed K_L^O decays originating in a neutral beam of well defined time structure. Decay products were detected by arrays of scintillation counters and wire spark chambers, positioned on both sides of a momentum-analyzing magnet. The counters serve both to identify events of interest, and to provide timing information for the charged particles. Photons and electrons were identified by their characteristic shower following one of several thin lead sheets, and muons by their penetration of the lead wall at the rear. Data acquisition logic was monitored by a PDP-9 computer which transferred the data to magnetic tape for later analysis. This apparatus has previously been employed in several other experiments, and more complete descriptions have been published in Refs. 73-76. Figures 3 and 4 show details of the layout and apparatus.

A. The K_L^O Beam

The K^O beam was produced by a 19.5 GeV electron beam incident on a one radiation length beryllium target. The secondary beam emerged through a hole in the 6 m thick shielding wall at an angle of 50 mrad with respect to the primary electrons. The beam port was blocked with 20 cm of lead to remove photons, and 163 cm of polyethylene to reduce the neutron contamination. During the data taking, a fire in the beam dump melted a portion of this polyethylene. After replacement, the final configuration was 30.4 cm Pb; 81.5 cm CH_2. The initial collimation was provided at 11.5 m from the target, and a second collimator removed scattered particles but did not intersect the beam. Charged components of the beam were removed by three sweeping magnets. In the center of the spectrometer magnet, the beam had a cross section 45 cm wide

by 30 cm high. Figure 3 shows the beam and collimation layout in End Station B.

The neutral beam was composed of K_L^O's and neutrons. The relative flux of kaons and neutrons was dominated by neutrons at low energy, was equal at roughly 4 GeV, and favored kaons at higher energies. The momentum spectrum of the K_L^O beam has been studied in some detail, and the procedure for extracting this spectrom is discussed in Ref. 68. The time structure of the K_L beam was very unusual, and provided a powerful constraint in this experiment. SLAC produces 360 beam pulses per second, each a maximum of 1600 nsec in duration. This structure is modulated by the primary 2856 Hz rf accelerating the beam so that each pulse is subdivided into fine structure "buckets" which are less than 5 psec wide. Near the injector, we superimposed a beam knockout system in which a 40 MHz oscillator swept out low energy electrons from our pulse, and allowed through only one bucket every 12.5 nsec. This separation was greater than the time-of-flight (TOF) difference between the fastest and slowest kaon of interest, and so allowed us to determine the production time for the kaon. A coaxial cable was mounted in the beam line immediately behind our target, providing a time reference signal (CABLE). By measuring the arrival time of the decay products with respect to the CABLE, we could determine the TOF of the K_L^O and thus its momentum.

B. Decay Volume, Counters, and Trigger Logic

The scintillation counters were arranged in seven banks (V, W, T/U, A, E, B, and C) as shown in Fig. 4. The dimensions of the counter hodoscopes are shown in Table 4. The V counter was viewed by four photomultiplier tubes (PMT's) to ensure high efficiency at rejecting charged particles, and was quite thin to minimize material in the beam line. An incident neutral was inferred

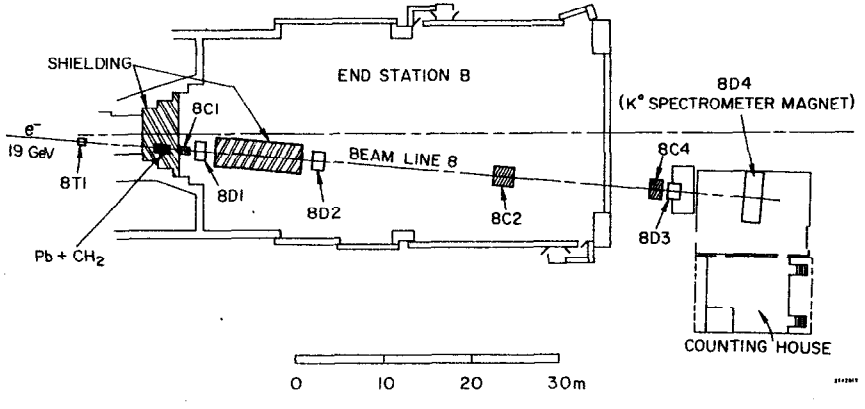

FIG. 3--Arrangement of beam line 8 in End Station B at SLAC. The production target is shown as 8T1, while the beam defining collimator is 8C1. 8C2 and 8C4 are two other beam collimators, while 8D1, 8D2, and 8D3 are the sweeping magnets.

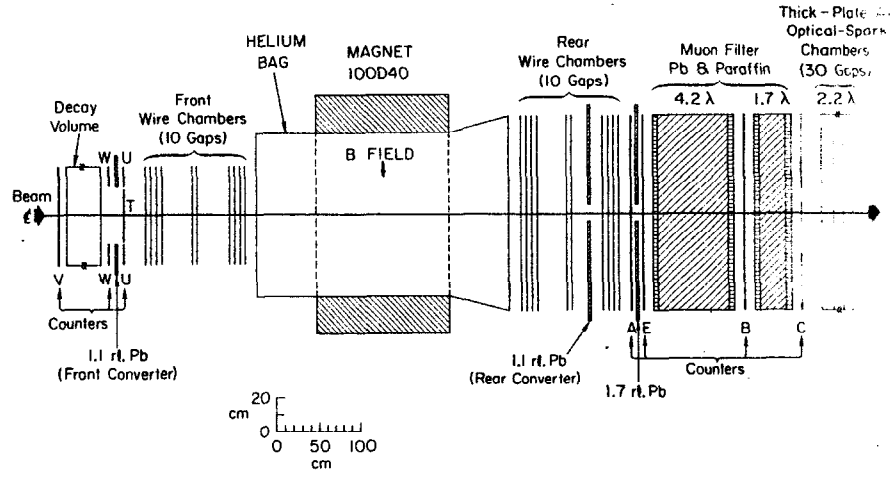

FIG. 4--Elevation view of the SLAC K_L^0 Spectrometer. The trigger requirement was $\overline{V}W\overline{U}2T2A$ or $\overline{V}2T3A$. Lead sheets for gamma and electron conversion are located between the W and U counters and upbeam of the A counters. λ represents absorption lengths. The E counters and optical spark chambers were not used in the analysis.

Table 4

Counter Hodoscope Dimensions

Hodoscope Bank	Area Covered (X, Y)	Each Counter (X, Y, Z)	Phototubes/Counter	# Counters
V	40" × 18"	40" × 18" × 1/4"	4	1
W	48" × 11"	24" × 11" × 1/2"	1	4
T/U	48" × 48"	24" × 2" × 1/4"	1	48
A	97" × 48"	6" × 48" × 3/8"	2	16
E	96" × 56"	48" × 11" × 1/2"	1	8
	(minus 24" × 12" hole in center)	36" × 6" × 1/2" (central counters)	1	14
B	85" × 66"	6" × 66" × 3/8"	2	14
C	97" × 66"	6" × 66" × 3/8"	2	16

from the absence of a signal in the V ($\overline{V}$). Between the veto counter and the T/U bank was a decay volume filled with helium to reduce the contamination from beam interactions. Material in the entire upstream portion of the spectrometer was minimized to prevent losses of resolution due to multiple scattering after the decay. The T/U bank was an array of 48 counters, each viewed by a PMT at one end. Immediately in front of the U counters were mounted W counters followed by a 1.1 radiation length sheet of lead. A fraction of the wide-angle gammas converted in the lead between the W and U bank, signalling their presence by a $\overline{W} \cdot U$. Signals from the T bank indicated charged particles emerging from the decay volume. Two charged tracks gave a signal 2T, where for purposes of notation, 2T implies a signal from two or more T PMT's. If these particles passed through the magnet, they were recorded by the A counters. The A, B, and C counters were viewed by a phototube at each end, were defined to have fired only if the signal from both tubes was present simultaneously. 2A, 2B or 2C implies in this case that two or more counters had both ends fired. Fifty cm upbeam of the A bank was a 1.1 radiation length lead sheet, with a hope cut in its center to pass the beam. The more forward photons traversed the magnet and converted in this sheet, and the resulting showers gave rise to additional A counters. Thus the logic signal for normal running was CABLE$\cdot\overline{V}\cdot 2T\cdot 2A\cdot(3A+\overline{W}\cdot U)$, where the two charged tracks following an incident neutral are indicated by $\overline{V}\cdot 2T\cdot 2A$, and the presence of a shower is inferred from either $\overline{W}\cdot U$ or 3A.

Many electrons shower in the same lead sheet, and roughly half the triggers contained an electron shower with no photon present. An additional lead sheet was located between the A and E counters. Electrons which did not

shower in the first sheet had the opportunity of showering and revealing their identity through additional pulse height in the E bank. Muons were identified by their ability to penetrate through to the B and C banks.

Timing information was read out into analog to digital converters (ADCs) from the U/T, A, B and C banks. The A counters provided the principal determination of the TOF for the event, and were equipped with XP1021 phototubes for superior time resolution. All the other counters were viewed by 56AVPs. For the A, B and C counters, the signals from both tubes were averaged by summing the output of each of their discriminators into a capacitive ramp. The integral of the summed signal was then fed into a third discriminator having a threshold set just above the output of one PMT alone. The time of this output signal was then independent of the position of which a particle struck the counter and statistically better defined than the time for one PMT alone. Latch information for every counter was recorded as well as pulse height information for the A and E counters. The high voltage on the A counters was adjusted so that a minimum ionizing track would produce a pulse height 8-9 times the discriminator threshold. This reduced the effects of time slewing due to pulse height variation. The E counter high voltages were set at roughly five times threshold to improve their dynamic range and provide a means to distinguish electrons from pions. The magnetic field at the T and A counters was no higher than 15 gauss, and their magnetic shields protected the tubes so that the pulse height varied by less than 5% the field polarity of 8D4 was reversed.

C. The Wire Spark Chamber System

Two sets of 10 gap wire spark chambers were placed on opposite sides of the spectrometer magnet to provide accurate determinations of the particle

trajectories. Each gap measured spark positions with respect to one direction, and the group of 10 gaps consisted of 4X's, 4Y's, one U and one V. (Our coordinate system has Z the beam direction, X horizontal, Y vertical, and U/V tilted in the XY plane.) The upbeam chambers were 1.2 m square, and the downbeam chambers were 1.2 × 2.4 m. In each case, the U and V planes were somewhat larger to cover the area completely. The system contained a total of 30K readout wires, each wire having diameter 0.1 mm, and a spacing of 1 mm. The chambers were read out through a capacitor-diode system. When the chamber was pulsed, a spark jumped along the path of ionization from a plane of individually isolated high voltage wires to the parallel readout wires at ground. A 1 nf capacitor was connected to each readout wire which collected the charge in the spark for later interrogation. This system led to very high multitrack efficiency; the chambers were able to handle hundreds of sparks at once, allowing us to reconstruct gamma and electron showers.

D. The Spectrometer Magnet

The momentum analyzing dipole (8D4) had an aperture 2.5 × 1 × 1 meter which was filled with a helium bag. Magnetic mirrors on both sides reduced the fringe fields. The experiment was conducted at a field integral of 12.6 kGm which imparted a transverse momentum kick of 377 MeV/c. An NMR probe monitored the vertical component of the field during operation. The reconstruction program employed a field map containing measurements of the three components of the field at 36,000 points on a grid 10 cm × 2.5 cm × 2.5 cm.

E. The Lead Wall and Optical Chambers

The lead wall had two sections, the first 75 cm thick and the second 30 cm thick. The minimum energy required for a muon to penetrate the first wall was 1.3 GeV, with 1.6 required to reach the C bank. Spurious counting in the

A counters from neutrons scattered back off the lead was reduced by installing parafin slabs between the E counters and the lead. The optical chambers were intended to provide additional muon momentum information in the search for the muonic rare decay candidates. After the kinematical analysis, no events remained as candidates, and the information from the optical chambers was not employed.

F. The On-Line System

The on-line system consisted of a PDP-9 computer with 24K of core. Its primary function was to record the data onto magnetic tape for off-line analysis. In addition, the computer monitored several of the hardware systems. Periodically the high voltage settings for the PMT's were checked, and miscreants were reported to the experimenters. The light diodes in the scintillation counters could be pulsed under computer control, testing the phototubes and related electronics. Before each run, the computer checked each wire in the readout system to determining if it would read ON when its capacitor was charged, and OFF after being cleared. Various histograms could be displayed (such as the numbers and positions of sparks, spark widths, latches, times and pulse heights) enabling the experimenter to spot malfunctions quickly. Individual events could be viewed showing all the sparks and counters. Histograms from old runs were saved on tape, and could be compared with the current status to search for long term variations in the spectrometer's performance. In addition, periodic off-line checks were run to monitor the wire chamber efficiency in detail.

G. Data Collection

Normal data collection interspersed with timing calibration runs occupied the greatest portion of the running time. In addition, several sorts of

specialized tests were made to determine geometrical constants and efficiencies. Each output tape contained a set of timing calibrations and one or more files of data.

1. Normal Running

As discussed above, the normal trigger requirement sought to isolate events containing two charged tracks before and after the magnet, plus a shower either upbeam in the U counters or downbeam in the A bank. Only about half the events written onto tape contained two full tracks, the remainder having the trigger satisfied by some accidental . The primary contributors were $K_L \rightarrow 3\pi$ with one of the photons from the π^o decay converting, or $K_L \rightarrow \pi e \nu$ with an electron shower giving the additional A counter. A data run usually lasted several hours filling one output tape with about 50K triggers.

2. Muon Runs

Muon runs determined a set of timing reference constants for each A PMT, the number of ADC counts required for a particle at v=c to travel from the target to the counters. For this running, the sweeping magnets were turned off, and the trigger changed to select straight-through tracks. For the central 12 A counters, we required that the muons penetrate to the B and C banks, thus selecting sufficiently high muon energies that energy dependent variations in TOF were minimized. This trigger was CABLE·V·T·A·B·C. Unfortunately, the outside two A counters on each side did not have B counters directly behind them, therefore we took another "special mu" run using a trigger CABLE·T·A allowing only these A counters. The flight path for these muons was not straight and no selection of muon energies was possible, therefore a correction to this calibration was made later in software when kinematic information provided an independent determination of the correct time. The flux without

the sweeping magnets was quite high, therefore the wire chambers were not fired during muon runs. A normal muon run collected $(0.3\text{-}2) \times 10^3$ events for each ADC, and a special run collected some $(1\text{-}2) \times 10^3$ in the outside counters.

3. Pulser Runs

The pulser runs determined another timing constant, the number of ADC counts corresponding to a known time interval. Under computer control, the light diodes in the counter banks were pulsed in combinations so that artificial events were generated. A substitute CABLE signal was used, since this run was not associated with the beam. Midway through the 2400 event run, the computer inserted a delay of 7 nsec into the dummy CABLE making the counter times appear 7 nsec earlier. The change in the ADC values for this time shift gave the ADC scale factor. The pulser run automatically checked that the photomultipliers and electronics were functioning and printed out diagnostic messages if the system malperformed.

4. Other Runs

A small fraction of the data was taken with a copper regenerator inserted in the decay volume. The veto counter was then moved behind the block to eliminate charged secondaries from interactions or K_S decays within the copper. The decay $K_S \rightarrow 2\pi$ is heavily overconstrained (3C without timing information), allowing us to accurately determine the resolution and alignment of the apparatus. We select two charged tracks via a trigger CABLE·$\bar{V}$·2T·2A.

Some 100K events were also taken with a 2.54 cm thick carbon block installed at several positions in the beam path. This particular block had 42 times the mass of the helium in the decay volume, and because the nuclear

properties of carbon and helium are similar, we thereby studied the effect of beam interactions on our normal event trigger.

Another segment of data (about 150K triggers) was taken under normal running conditions, but without the shower requirement, so that we would have an internal consistency check of our gamma conversion efficiency calculations, as discussed in Section IV.

Finally, we took 65K triggers under all normal running conditions, but without the lead sheet in front of the A counters. This data enabled us to refine the shower-finding software and reduce background processes generating spurious gamma showers.

III. DATA REDUCTION

The current K^o spectrometer differs from its predecessors by employing many more detectors, and consequently has available a great deal more information concerning each event. The profusion and precision of our information enabled us to detect, identify and measure contaminations which would otherwise have been estimated.

A. PASS 1

PASS 1 had several major responsibilities: to reconstruct the track segments from the spark addresses; to locate the conversion points of showers, and to calibrate the time ADC's.

1. Track Reconstruction

The wire chambers provided 4X, 4Y, and a U and V spark for each upbeam and downbeam track segment. The use of 10 gaps to determine a three-dimensional line segment provides a high degree of redundancy, and enables the system to locate tracks in the presence of background and occasional chamber inefficiency. The object here was to find every straight line formed by 3 or 4 sparks. For each X segment that was found, a best-fit slope, intercept, and χ^2 were computed. Such an X segment could contain accidental lines formed by combinations of sparks having nothing to do with true particle paths. To reduce these accidentals, we compared the χ^2 of lines sharing sparks, and discriminated against the poorer χ^2. Having found all such X segments, the same procedure is applied to find the Y segments. Since the U and V planes are linear combinations of X and Y, the ambiguity of which X segment is to be associated with a given Y segment is resolved by comparing the projection of the X and Y segments into the U and V planes with the existing sparks in these planes. Accidental coincidences in the U/V planes are handled by the same χ^2

procedure as for the X and Y planes. Each front and rear track had a slope, intercept and χ^2 written onto the output tape.

2. Shower Finding and Electron Identification

To detect photons and electrons, we modified the spectrometer by adding two 1.1 radiation length lead sheets as shown in Fig. 4. These were arranged so that they did not intercept the beam, however a given photon or electron passed through only one sheet, thus the conversion efficiency was limited to about 47% for gammas and 55% for electrons. We attempted to distinguish electrons from pions by means of a third 1.1 radiation length lead sheet inserted between the A and E counters. Electrons which did not shower in the first sheet would be indistinguishable from pions, however if they showered between the counter banks, an abnormally high pulse height would be recorded at the E bank. In this experiment, the correlation between leptonic events and high E pulse height was not adequate to identify electrons and was not used.

In the front chambers, shower elements emanating from the lead pass through the wire chamber system and are located as track segments. In the rear, they pass through only two X and two Y planes and are thus not normally located by PASS 1 as tracks. The shower-finding software made use of a very intuitive approach: The X and Y centroids are located independently by forming lines through pairs of sparks in the two chambers. All the possible lines connecting a spark in one plane with every spark in the other were constructed. For real showers, lines from several shower elements converge at a single point at the lead sheet, while for accidentals there will be no such grouping. Naturally, a great many such lines were possible, and to reduce the accidentals, we demanded that each segment point at a photomultiplier that fired in the event, and that the slope of the line not exceed 45° relative to the Z axis. The line

segments corresponding to shower candidates clustered at the plane of the lead. In general, even a good shower could have several accidental clusterings, however these separate groupings would share common sparks. The best cluster for the shared sparks was then chosen on the basis of the number of elements contributing and the deviation from the centroid. After a shower had been found, the already-used sparks were then eliminated from further consideration, and those remaining were again tested. In general, a different number of clusters in X and Y could be found, and it remained to match a given X with its proper Y. In the front, this was done by using the association provided by the U/V sparks for the line segments. In the rear this information was not available. Since the A counters were equipped with a PMT at each end, the time difference between these two tubes was proportional to the vertical position of the track striking that counter. Therefore, each X conversion point had a certain Y from the A timing, and this was matched with the Y conversion found by the grouping.

Electrons are identified by the presence of a track incident on the Pb sheet and a shower emerging behind. Usually one outgoing element had the same direction as the incoming electron, however various other categories of electron showers were observed, including showers which converged a short distance from the point at which a track passed through the lead. These were tentatively tagged as electrons when they converted within 5 cm of the track's projected intercept.

For a shower to be written onto output tape, the software had to locate at least one grouping in both X and Y which was consistent with the latch and timing information. If there was no corresponding incident track, the shower

was passed as a photon. If an upbeam track pointed through the shower, then the track was identified as an electron and the shower was not passed.

The spatial resolution as shown in Fig. 5 was determined using the shower-finding routines to locate showers that were known to be electrons. By examining the distance between the projected electron intersection and the shower conversion point, we found the shower resolution in the rear to be ± 3.4 mm in both X and Y. Electrons were not identified for upbeam showers, however a comparison of the conversion point with the projected intersection point of a track segment from the shower gave the resolution in front as ±1.25cm in both projections.

Calibrations of the time ADC's: Each time ADC measured the overlap of a gate generated by the CABLE signal with the output of a particular counter through a discriminator. We needed two constants to convert the ADC counts to usable information: one to set the scale factor for the counts per nsec, the other to establish the ADC value corresponding to a known time measurement. As mentioned in the description of a Pulser Run, the computer selected various combinations of PMT's and repeatedly pulsed their light diodes. Halfway through this operation, a delay of 7 nsec was inserted into the pulser timing signal, thereby changing the overlap of the PMT signal and gate. The ADC scale factors are then computed from the difference in counts corresponding to the 7 nsec delay. It remained to bring all the individual ADC's into one uniform scale of reference. Using muons (essentially at v=c), we establish one constant for each ADC corresponding to the arrival time of a v=c particle. It sometimes occurred that an insufficient number of events were taken and in this case, the calibration constants from the immediately previous run were used. These were then updated at the next adequate muon

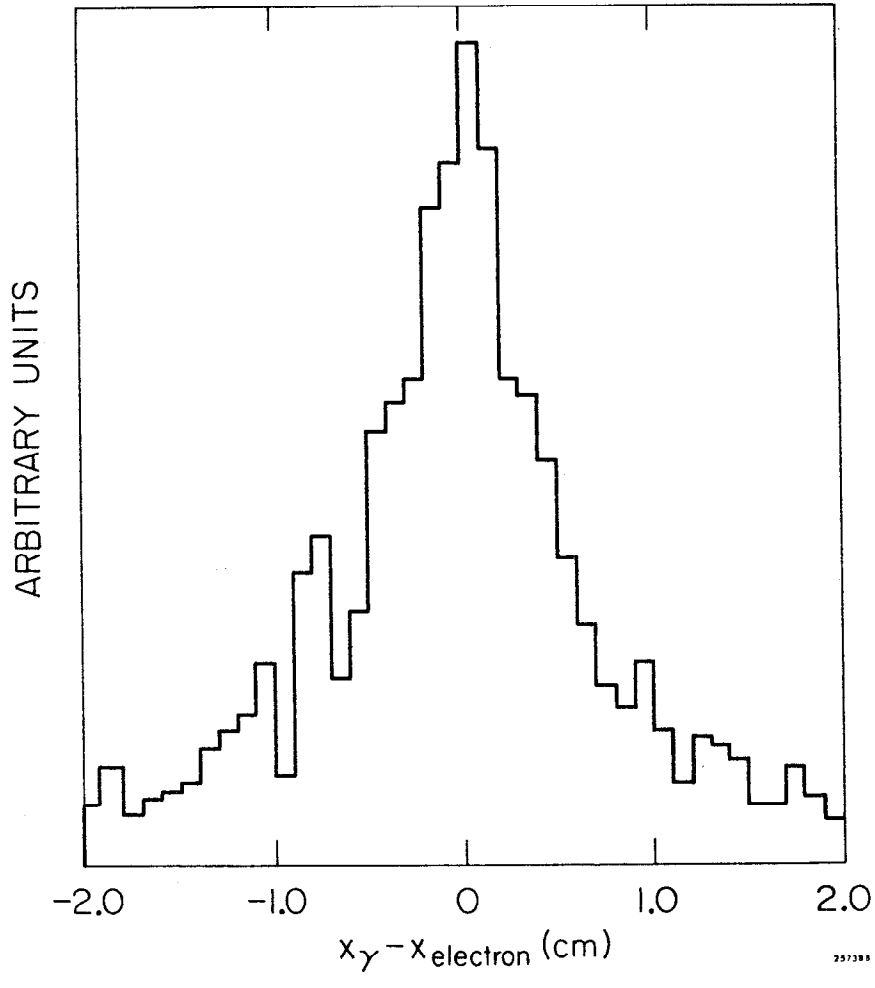

FIG. 5--Shower reconstruction resolution. $x_{electron}$ is the projected intercept of an electron at the lead sheet; x_γ is the conversion point of the resulting shower.

run. Several sources of variation remained, and were corrected after PASS 2 when kinematics could be used to select events with a known time to compare with these measurements.

B. PASS 2

PASS 2 matched the track segments through the spectrometer magnet, computed their momentum, and found their vertex. In addition, a subprogram identified penetrating muons.

1. Track Matching Through the Magnet

An ideal track had its upbeam and downbeam X line segments intersect near the magnet's midplane, and the same Y slope and intercept on both sides of the magnet. The difference in the X direction cosines then determined the momentum. In reality, effects such as vertical focusing degraded these conditions somewhat, however since each potential pairing must satisfy four equations relating the direction cosines to the one unknown momentum, there are three constraints. Fortunately, the horizontal momentum transfer was virtually independent of the trajectory, so that each pair (consisting of one upbeam segment and one downbeam segment) had an approximate momentum computed from the horizontal bend angle. Vertical focusing corrections were then applied to the Y direction cosines, and the candidate was integrated through the field map using the approximate momentum. If the integrated trajectory was consistent both with the position and direction of the downbeam segment, the track was deemed matched. A final refined momentum was computed using the integrated direction cosines. Finally, the upbeam direction cosines were corrected for bending in the fringe field in the front chambers. Charged decay products originated from a point vertex, however after reconstruction the line

segments in general did not converge precisely. The vertex was then defined to be the average of the track positions at the point of closest approach.

2. Muon Identification

Muons were identified by their ability to pass through the lead wall. All tracks having an energy greater than the minimum necessary to pierce the initial 79 cm lead wall (at their particular incident angle) were candidates, and a search was made for B and C counters associated with that track. Due to the effects of multiple scattering, the latches were accepted if there was a counter within a reasonable distance of the projected horizontal intercept of the track at the counter plane. In addition, the time from the struck counter was required to be consistent with the corresponding time at the A bank. Tracks were flagged as muons having either an AB latch, or an ABC latch. A muon could not be identified if it had p_μ less than 1.3 GeV/c, however, above this momentum the muon detection efficiency is very high ($\sim$90%), and we identify approximately 70% of all the muons. A fraction of the pions impinging on the lead wall punched through to the downstream counters, while other pions generated real muons by decaying in flight. From a study $K_L \rightarrow 3\pi$ events with a muon found, we estimate the probability per pion to penetrate by either means is $\sim$7%.

3. Mortality in PASS 1 and PASS 2

Not all events written by the PDP-9 survived this initial analysis. In PASS 1, the only way events could fail was by having $\geq$ 24 sparks in one or more planes, which eliminated 3-5% of the data. In PASS 2, the event was required to have two full tracks which verticized. Fully 50% of the events failed, through having too few matched segments in the front or rear, or no

vertex. Beyond this point, the events were specially selected onto various summary tapes.

C. Timing Corrections

After timing calibrations had been done in PASS 1, several corrections remained that required a knowledge of the true event time. We determine the true time for an event by reconstructing the kaon momentum from the measurements of the charged momenta and directions, the particle masses, and the K_L^o direction. This experiment constantly made reference to a $K_{\pi 3}$ data sample where the kinematic behavior is well understood, and there are copious events available. The traditional means of isolating this decay involves the variable $p_0'^2$, which is the momentum of the kaon (squared) in the frame where the sum of longitudinal components of the charged decay products is zero.

$$p_0'^2 = \frac{\left(m_K^2 - m_{\pi\pi}^2 - m_{\pi^o}^2\right) - 4\left(m_{\pi\pi}^2 m_{\pi^o}^2 + m_K^2 p_\perp^2\right)}{4\, m_{\pi\pi}^2 + p_\perp^2}$$

where $p_\perp$ is the sum of the transverse momenta of the charged decay products. This variable does not depend on the measured timing information, and is very sensitive to a misidentification of the particle masses, as well as the maximum transverse momentum of the decay. For this reason, $p_0'^2$ is always computed assuming a $K_{\pi 3}$ decay. In the absence of resolution errors, $p_0'^2$ is positive for a $K_{\pi 3}$ decay. In contrast, most $K_{\ell 3}$ decays reconstruct negative $p_0'^2$ as shown in Fig. 14.

The reconstruction of the momentum of the kaon in the laboratory results in two solutions due to a quadratic ambiguity corresponding to forward and backward emission of the π^o in the kaon's center-of-mass frame. The true time is determined by selecting a sample of $K_{\pi 3}$ events in which the ambiguity

corresponded to a calculated time difference less than 100 picoseconds. This class of events arises when the transverse momentum is a maximum, and the true time is taken to be the average of the two solutions. We compared the measured time to this reference time as a function of several variables which affected the measured time.

The apparatus measured the time of arrival of decay products with respect to the arrival time of the beam. The beam deposited charge in a coaxial cable mounted behind the target, and this signal was passed through an amplifier to a discriminator (CABLE) whose output generated the timing gate. The event's measured time is formed from A counter timing information for path charged tracks and photon showers. The A counters had a photomultiplier tube at each end, both of which have an individual discriminator. The outputs of these two discriminators are then summed into a capacitive ramp circuit. The integral of the summed signal is then fed into a third discriminator having its threshold set just above the output of one PMT alone. The time at each A counter is proportional to the overlap of the counter's discriminator output with the output from the CABLE discriminator.

We studied timing variations arising from changes in the pulse height into the CABLE discriminator, from miscalibration of individual A counters, and from variations in A counter pulse height for both showers and tracks.

1. Cable Pulse Height

The variation of the time recorded by the A counter as a function of CABLE pulse height is shown in Fig. 6a. We apply a correction of 12 picoseconds per ADC channel.

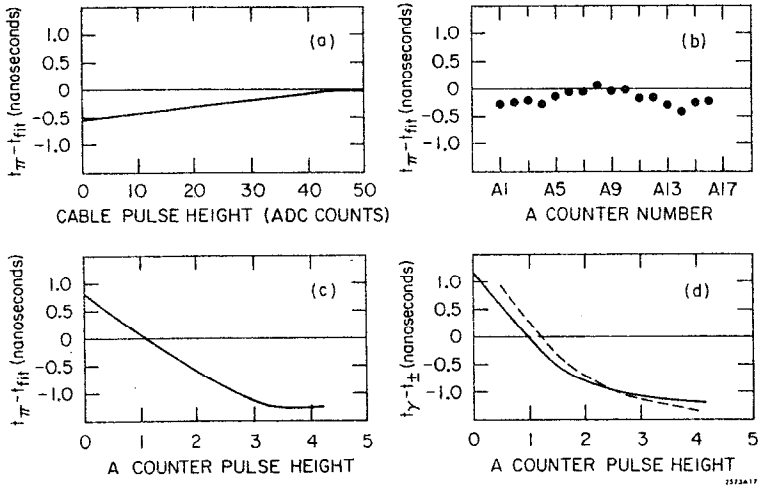

FIG. 6--Timing corrections. (a) Variation in charged track time as a function of CABLE pulse height. t_{fit} is the kinematical timing solution for $K_{\pi 3}$ events in which the quadratic ambiguity for p_K corresponded to time differences less than 100 picoseconds. (b) Variation in charged track time in each A counter for a particular run. Each run is corrected independently. (c) Variation in charged track time as a function of A counter pulse height, shown here in units of minimum ionizing pulse height. (d) Variation of gamma time (rear only) as a function of A counter pulse height. Solid curve is for showers striking only one A counter; dotted curve is for multiple counter showers. $t_\pm$ is the average of the two charged track times after corrections (a) - (c).

2. Individual A Counter Recalibration

PASS 1 timing calibrations are based on the assumption that muons travel a straight path from the target to the counters. This is not true, particularly for the outside A counters, or if a sweeping magnet is left on during a muon run. Individual runs differed substantially, and an appropriate correction was applied for each counter and run, thus removing all run-dependent effects as well as possible DC shifts in the calibration. A typical correction is shown in Fig. 6b.

3. Pulse Height Slewing in the A Counters

Pulse height variations in the counters change the relative time the counter's discriminator fires, thus modifying the overlap with the timing gate. PASS 1 assumed a minimum ionizing pulse for the muons, however much of the data included more heavily ionizing particles such as electrons or low energy pions. The pulse height timing variation is shown in Fig. 6c for charged tracks. Photon showers differ from normal tracks in that several shower elements are present and may impinge on more than one A counter. If more than one element strikes a given A counter, each phototube records the arrival of the first light to reach it, making the resulting time appear earlier by an amount proportional to the spread of the shower. Several different cases are possible, depending on the number of A counters and shower elements involved. Figure 6d shows the time slewing for each case. After correcting each A counter in the shower, their times are averaged to give the final gamma time.

Gammas are also detected in the front counters, for which no PASS 1 reference time exists, so that each U time ADC must be calibrated by a comparison with the average time of the charged tracks, and a set of U counter

offsets generated. Since the time resolution in front is poorer than in the rear, one set suffices for the entire data. Finally, since each U counter has only one PMT, a correction is required for the transit time of photons from the X intercept of the particle to the photocathode. As in the rear, multiple counter showers are averaged.

The result of all these corrections is to reduce each effect to a deviation of less than 100 picoseconds with respect to the true time. This enables us to reject events having internal inconsistencies wherein either particle or the photon were significantly out of time. The time resolution for the two charged tracks alone was 0.3 nanoseconds; when the showers are included it is 0.25 nsec. See Fig. 7 for various timing resolution curves.

D. PASS 3

PASS 3 completed the kinematic reconstruction of the data and histogrammed a large number of variables. These plots displayed the types of events comprising the summary tapes, and from them suitable criteria were determined for the isolation of a particular decay mode. Section V contains a discussion of the analysis procedures in detail.

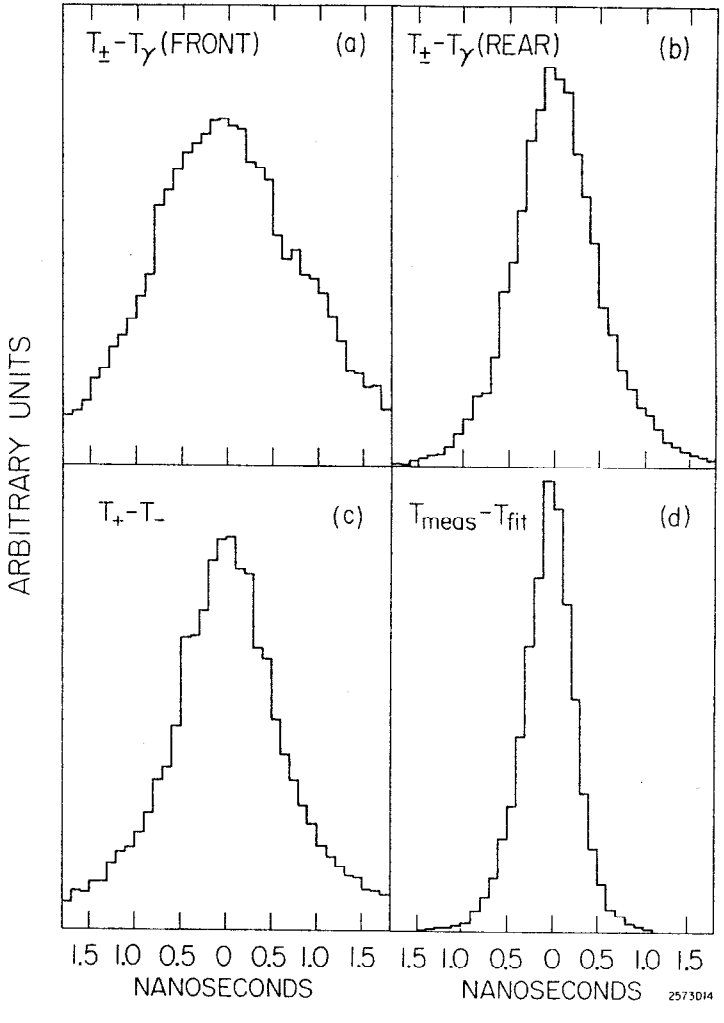

FIG. 7--Timing resolution. (a) Front showers. (b) Rear showers. (c) Charged track times. (d) Overall average $t_{meas} = \frac{1}{2}(t_{\gamma}(REAR) + t_{\pm})$. $t_{\pm}$ is the average of the two charged track times. t_{fit} is the actual event time determined kinematically.

IV. CALIBRATIONS AND NORMALIZATION

A. The Monte Carlo

The objective of the Monte Carlo program was to compute the detection efficiency for many decay modes, and to provide a basis of comparison whereby systematic effects in the apparatus and background contaminations could be isolated. For example, the decay $K_L \rightarrow \pi\pi\gamma$ necessitated generation of $K_{\pi 3}$ for normalization and background studies, as well as K_{e3} and $K_{\mu 3}$.

In the case of $K_{\mu 3}$ and $K_{\pi 3}$, the matrix elements for the decay are relatively well known, and the recent results[77,78] from this apparatus were employed. However, the processes for the rare decays are unverified, and the various model-dependent matrix elements will be discussed concurrently with the particular decay.

Many Monte Carlo simulations only record the relevant details of events remaining at the final stage of the analysis, however this shortcut does not allow a continuous comparison of simulated and real data at each stage of the reduction process. Much of the analysis software was modified to accommodate this experiment, and sundry anachronisms remained which could only be located via a detailed and careful comparison. Accordingly, the output of the Monte Carlo consisted of artificially generated raw data tapes with the same spark and logic information as written by the PDP-9. Subsequent analysis of these events paralleled the real data from PASS 1 to PASS 3.

1. The K_L^o Beam

A major problem in any experiment employing a neutral beam is the determination of the beam spectrum. The beam was identical to the earlier charge asymmetry and form factor experiment (E-64), so that the spectrum (Fig. 8) had already been extracted from the distributions of charged pion energies in

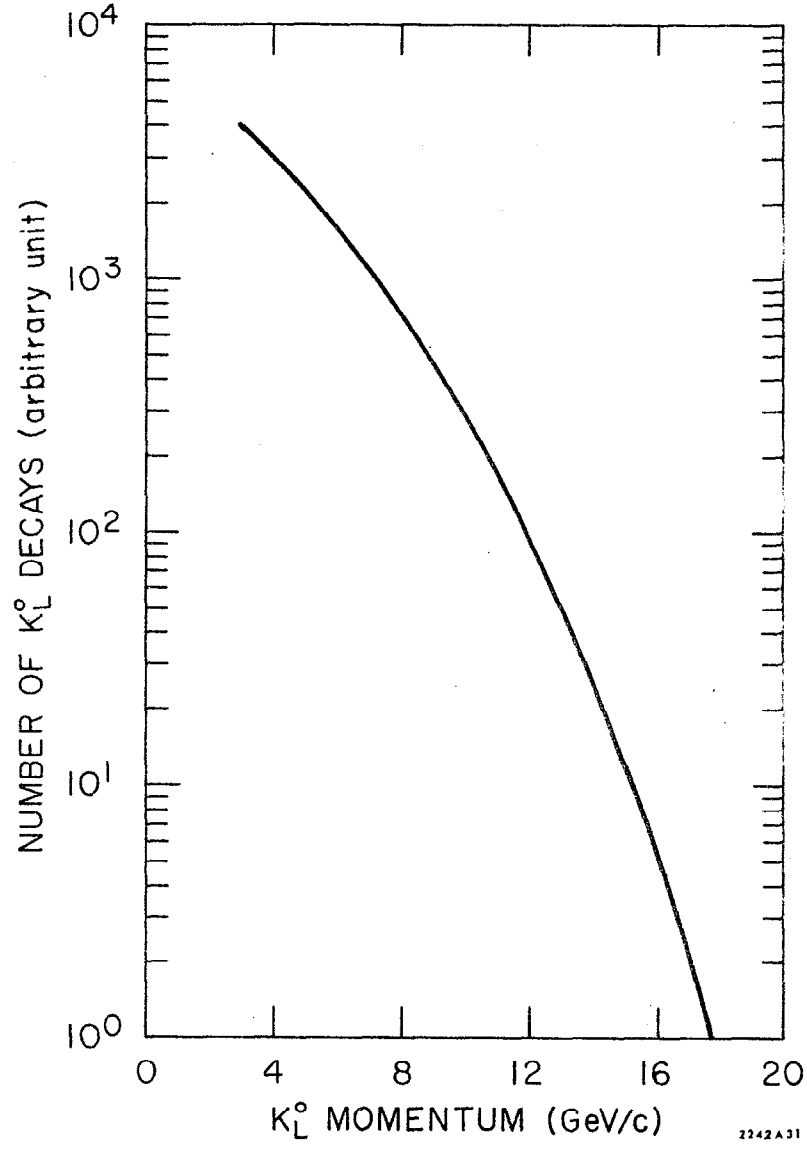

FIG. 8--K_L^o decay momentum spectrum.

$K_{\pi 3}$ decays taken at that time. A complete discussion of this technique is given in Ref. 78; for completeness, a brief outline follows. An appropriate mixture of $K_{\pi 3}$, $K_{\mu 3}$ and K_{e3} decays had been generated, passing the same cuts as the data. $N(E_{\pm}, P_k)$, a matrix describing the shape of the $E_{\pm}$ spectrum as a function of the kaons laboratory momentum was determined from these events. The shape of the K_L^o decay momentum spectrum, $F(P_K)$ was then determined from the matrix equation $F=N^{-1}W$ where $W(E_{\pm})$ is the experimentally observed $E_{\pm}$ spectrum. This procedure did not depend on TOF measurements. The accuracy was about 2% at the peak, worsening due to poor statistics to about 10% at very low and very high P_K.

2. Beam Scattering

The beam port was blocked with lead and polyethylene to remove photons and neutrons, therefore a substantial number of kaons were diffractively scattered before reaching the apparatus. A rough calculation indicated that approximately half the kaons scattered, therefore half the Monte Carlo events were generated with the kaons coming from a point target, and the other half from an extended source at the collimator.

We extracted the magnitude of the scattering empirically using a sample of $K_{\pi 3}$ events with two photons detected. Assuming the masses, and having the charged directions and momenta as well as the photons' directions, it is possible to reconstruct the direction of the kaon. For the data the difference between the calculated K direction and the measured had a FWHM of 2.1 mrad for both X and Y. The Monte Carlo sample without K scattering had widths 1.8 and 1.9 respectively, and the collimator-sized target produced 2.8 and 2.0. Averaging these two samples therefore produced a reasonable approximation to the observed scattering.

3. Wire Chamber and TOF Data

Each charged particle was traced through the magnetic field, and the wires closest to its trajectory were recorded. Each spark was given a Gaussian jitter of width 0.35 mm about its true position to reproduce the observed distribution of the distance of a spark along a track from the best fit line through all the sparks in the track.

The Monte Carlo was made to duplicate the latch and ADC information in the data. For each charged track, a TOF was computed along its path from the decay vertex to the counters. The kaon TOF from the target to the vertex was added to this time, and the time for a v=c particle was subtracted. The times for each of the two phototubes (one phototube for the U and T counters) was then converted to an ADC reading, using the average scale factor of .135 nsec/ADC channel. It was difficult to reproduce the experimental timing resolution in the Monte Carlo due to contaminations from several sources: Additional tracks could pass through the same counter within the timing gate, either from showers (both real and accidental) or resulting from the neutron splash in the lead wall. In the apparatus, if two tracks passed through the same counter, the phototube recorded the first light that reached it. This resulted in erroneous TOF measurements for the real tracks, since the light would reach one tube early, and the pulse height would be abnormally large. The Monte Carlo reproduced this effect for decay products, however, background tracks from accidentals or from the neutron splash in the lead were not included. In addition, the shower elements were generated in a somewhat unphysical way (see following section) and did not reproduce the timing characteristics of actual showers. No internal consistency requirements were applied to Monte Carlo times, as this cut was intended to remove

spurious triggers from real data. To a good approximation, these effects were random, and a gaussian jitter of 0.3 nanoseconds was applied to each track time. We chose the fitted kaon momentum as the solution closest to the measured time, and this timing jitter in the Monte Carlo was necessary so that we did not bias the acceptances by choosing the correct solution more often.

4. The Gamma and Electron Showers

The essential principle in the simulation of showers was to produce 100% conversion and detection efficiency, in order that the determination of the actual conversion probability in the data would be free of special effects dependent on techniques used in generating the shower. Shower losses in Monte Carlo data would then be limited to the geometrical acceptance of the apparatus, and would not contain any of the complicated physics of shower propagation through the spectrometer. To this end, each electron and photon incident on a lead sheet produced two electron-positron pairs leaving the lead sheet. One particle continued forward along the incoming direction, and the other three diverged at 3(10) mrad in fron (rear), arranged symmetrically in the azimuthal plane. This construction virtually guaranteed that at least one shower element would be present in the chambers.

While this technique was useful to determine the shower conversion efficiency, the Monte Carlo showers did not reproduce the showers found in the data. These differences were negligible for purposes of extracting a branching ratio, however the data was later used in a $K_{\pi 3}$ Dalitz plot analysis which required systematic corrections for these discrepancies.

5. Muons

The earlier experiment on $K_{\mu 3}$ produced a good understanding of the identification of muons in the apparatus.[75] Since the muons have no hadronic interactions, the effects of multiple scattering in the paraffin and lead are accurately reproduced in the Monte Carlo. However, in addition pions may counterfeit muons in several ways and thereby contribute to the backgrounds expected in rare muonic decays. The decay $\pi \rightarrow \mu\nu$ produces actual muons which satisfy the criteria; also the pion could penetrate the wall without interacting, or the charged results of a hadronic interaction could trigger a B or C counter. Pion decays were ordinarily included at their normal rate ($c\tau$=780.2 cm), however pions "punching through" were not contained in the Monte Carlo, and this effect was estimated directly from the data.

B. Gamma Conversion Efficiency

The determination of the conversion efficiency involves not only the intrinsic ability of a lead sheet to initiate a shower, but also the ability of the programs to recognize various configurations of sparks as a shower. In addition, functional dependences on position and energy must be correctly taken into account, if we are to use the correct shower conversion probability in determining the normalization and acceptances.

To obtain the global conversion probability, the fraction of events in the data containing one or two showers was compared with the fraction observed in the Monte Carlo at unit conversion efficiency. In general, this could be different for front and rear showers, although the converter thickness is the same in both cases. We therefore perform the following calculation independently for front and rear showers:

Fraction of events with 0, 1, or 2 gammas in the data $\equiv N_0, N_1, N_2$

Fraction of events with 0, 1 or 2 gammas in the

Monte Carlo $\equiv M_0, M_1, M_2$

Shower conversion and detection efficiency $\equiv X$

where X may be X_F or X_R for front or rear showers.

Three equations link the observed fractions via the unknown conversion efficiency:

$$N_2 = X^2 M_2 \tag{1}$$

$$N_1 = XM_1 + 2X(1-X) M_2 = X(M_1+2M_2) - 2X^2M_2 \tag{2}$$

$$N_0 = M_0 + (1-X) M_1 + (1-X)^2 M_2 = (M_0+M_1+M_2) - X(M_1+2M_2) + X^2M_2 \tag{3}$$

dividing (2) by (1) gives

$$\frac{N_1}{N_2} = \frac{1}{X}\left(\frac{M_1}{M_2} + 2\right) - 2$$

or

$$X = \left(\frac{M_1}{M_2} + 2\right) \Big/ \left(\frac{N_1}{N_2} + 2\right) \tag{4}$$

Dividing (3) by (2) and setting $M_0+M_1+M_2 = 1$ gives

$$X\left(\frac{N_0}{N_1}\right)(M_1+2M_2) - 2X^2 M_2\left(\frac{N_0}{N_1}\right) = 1 - X(M_1+2M_2) X^2M_2$$

$$X^2\left[M_2\left(1 + 2\frac{N_0}{N_1}\right)\right] - X(M_1+2M_2)\left(1 + \frac{N_0}{N_1}\right) + 1 = 0 \tag{5}$$

In order for a shower to be considered, it must first satisfy several quality requirements; in particular that the conversion point lie within the boundary of the appropriate lead sheet (and not inside the hole through which the beam

passes in the rear sheet), and that its time information is consistent with the time measured for the two charged tracks. Spurious gammas originate primarily from π^o's produced in other K decays in the beam, and are not associated with the decay that triggered the apparatus. These are removed by the condition that $|T_\gamma - \left(\frac{T_+ + T_-}{2}\right)| < 1.0$ nsec in the rear and 2.0 nsec in front. Certain of these accidentals will fall within this time cut, and will thus distort the observed fractions N_0, N_1 and N_2. If we make the simplest assumption that there is a constant probability δ of having a random gamma (independent of the number of real gammas in the event), then the equations for the N's become (to order δ^2):

$$\begin{aligned} N_0' &= N_0(1-\delta) \\ N_1' &= N_0\delta + N_1(1-\delta) - N_0\delta^2 \\ N_2' &= N_0\delta^2 + N_1\delta + N_2(1-\delta) - N_1\delta^2 \\ N_3' &= N_1\delta^2 + N_2\delta - N_2\delta^2 \\ N_4' &= N_2\delta^2 \end{aligned} \tag{6}$$

where the N''s are the observed distributions, and the N's the original distributions, and we have kept terms to order δ^2, since we expect δ to be $\sim 10^{-2}$. Unfortunately, δ need not be the same in front and rear, so that it is necessary to solve for both δ_F and δ_R simultaneously:

If the true distribution is

NSR =	0	1	2
NSF = 0	P_{11}	P_{12}	P_{13}
1	P_{21}	P_{22}	
2	P_{31}		

where P_{11}, for example, is the uncontaminated fraction of events found in the data, having NSR=0 and NSF=0. And the true distribution:

	Zeroth order			order δ	order δ^2
NSR =	0	1	2	3	4
NSF = 0	Q_{11}	Q_{12}	Q_{13}	Q_{14}	Q_{15}
1	Q_{21}	Q_{22}	Q_{23}	Q_{24}	
2	Q_{31}	Q_{32}	Q_{33}		
3	Q_{41}				

where Q_{11} is the observed fraction of events found in the data, having NSR=0 and NSF=0. One may relate the observed fractions to the true fractions using δ_F and δ_R, from which we find $\delta_R = .026 \pm .003$ and $\delta_F = .0032 \pm .0009$. In principle, we could then recompute the true fractions and obtain the conversion efficiencies via Eqs. (4) and (5). However, the results of such a computation are quite sensitive to the exact choice of δ_R and δ_F, therefore we generated solutions to (4) and (5), varying the δ's.

We compute the weighted average of the 2T·2A data (N_0/N_1 method) and the 2T·3A data (N_1/N_2 method) at which the proper contamination (δ_F and δ_R) gives $x_F = 45.0 \pm 1.1\%$ and $x_R = 46.1 \pm 0.9\%$. Note that since we have required a shower in the trigger, we cannot employ the N_0/N_1 method for 2T·3A data. Also, very few events in the 2T·2A data have 2 showers, so that the N_1/N_2 method is very poorly determined. Finally, we have a consistency check directly in the 2T·2A data, where

$$N_1 = X(M_1 + 2M_2) - 2X^2M_2 \text{ from which } X_R = 45.01\%$$

$$N_0 = 1 - X(M_1 + 2M_2) + X^2M_2 \text{ from which } X_R = 46.41\%$$

which appears in good agreement with the averaging technique.

1. The Momentum Dependence of the Gamma Conversion Efficiency

We expected constant conversion efficiency at high momentum, however due to the physical behavior of showers and certain software criteria, this efficiency must fall off for low momentum gammas. To determine this behavior, we select only $K_{\pi 3}$ events which must also have two showers passing the quality requirements for the $\pi\pi\gamma$ analysis. As shown in Fig. 9, the intersection of a plane determined by the K_L and the charged transverse momentum with the plane containing the two gammas specifies the direction of the π^o. The momentum of the π^o is obtained from the conservation of transverse momentum. The angles of the gammas with respect to the π^o finally determine the momentum of each gamma. The ratio R = (number of gammas at p_γ in the data)/(number of gammas at p_γ in the Monte Carlo) gives a number proportional to the conversion efficiency as a function of momentum.

This method will not apply if the two gamma momenta are correlated, such that p_γ implies a particular p_{γ_2}. We check this using the original unperturbed values on the Monte Carlo tapes to compare with the reconstructed momenta, and within the accuracy available, no correlation exists. It may also occur that the two gammas did not originate in the π^o decay, in which case they will fail to reconstruct the π^o mass. We choose the mass cut to pass 90% of the Monte Carlo data, which depletes the region $p_\gamma < 150$ MeV for both data and Monte Carlo. Since few low momentum gammas remain, R is quite unstable below 150 MeV/c, however a check using as data Monte Carlo gammas with a known momentum-dependent conversion efficiency reproduces the low momentum spectrum accurately. We must also consider whether the method has sufficient resolution, since at very low momentum we expect the resolution to diverge: Consider that a gamma having low momentum in the lab

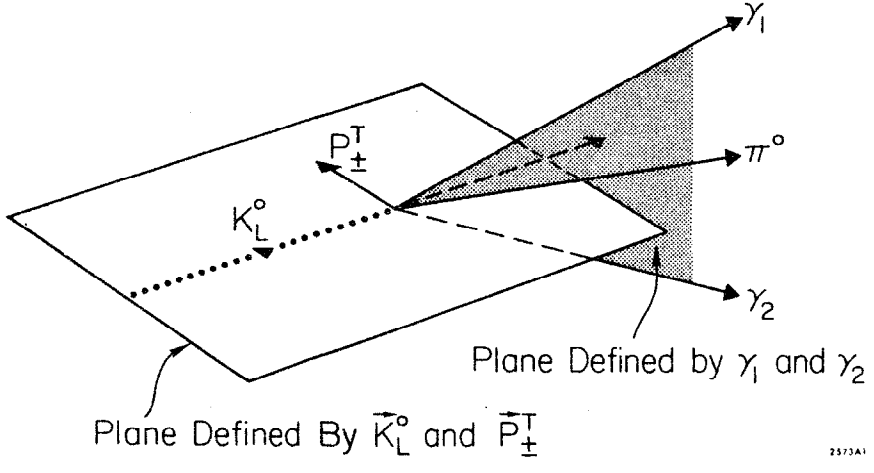

FIG. 9--Reconstruction geometry for $K_L^o \rightarrow \pi^+\pi^-\pi^o$ decays with two gammas observed.

system has likely been emitted backwards in the π^o c.m. system. In the lab, the gamma energy is

$$E_\gamma = \frac{\gamma_{\pi^o} M_{\pi^o}}{2} \left(1 + \beta_{\pi^o} \cos \theta^*\right)$$

and we take $\theta^* \simeq \pi - \epsilon$ (nearly backward emission), so that

$$\cos \theta^* \simeq - \cos \epsilon$$

$$\sin \theta^* \simeq \sin \epsilon$$

$$\beta_{\pi^o} \simeq 1$$

Then E_γ becomes:

$$E_\gamma = \frac{\gamma_{\pi^o} M_{\pi^o}}{2} (1 - \cos \epsilon) \simeq \frac{\gamma_{\pi^o} M_{\pi^o}}{2} \left(\frac{\epsilon^2}{2}\right)$$

and

$$\frac{\delta E_\gamma}{E_\gamma} = \frac{2\delta\epsilon}{\epsilon}$$

which blows up when the gamma goes backwards in the π^o system. Figure 10 shows the variation of resolution for various ranges of p_γ. As a test that this method works as accurately as possible, we find that the unperturbed direction cosines for the photons reproduce the gamma momentum exactly (even for low momentum gammas). We conclude that above 150 MeV/c, the momentum dependence of the conversion efficiency should be accurately determined.

Figure 11 shows the ratio R versus p_γ, from which we discern that the conversion efficiency is constant above 100 MeV/c.

2. Expected Conversion Efficiency

The underlying theory of photon-initiated showers is well understood, so that in principle one can calculate the probability of detecting a shower, given the incident energy and the thickness of the radiator. In practice, various

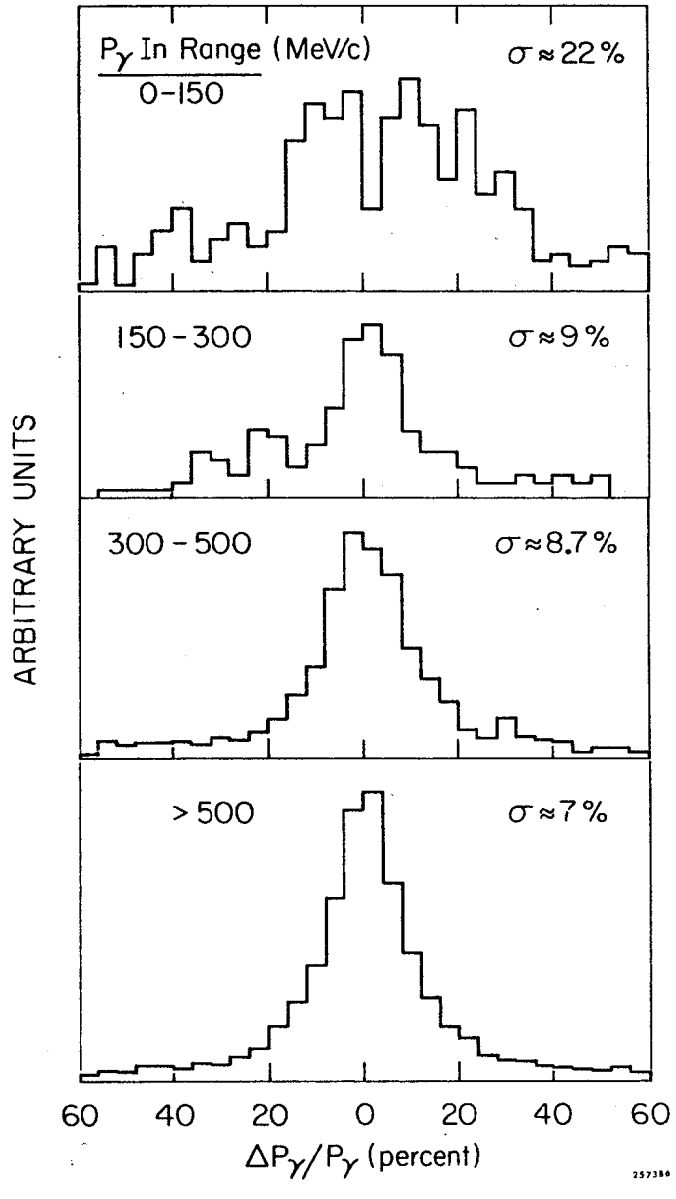

FIG. 10--Momentum resolution for two photon reconstruction technique.

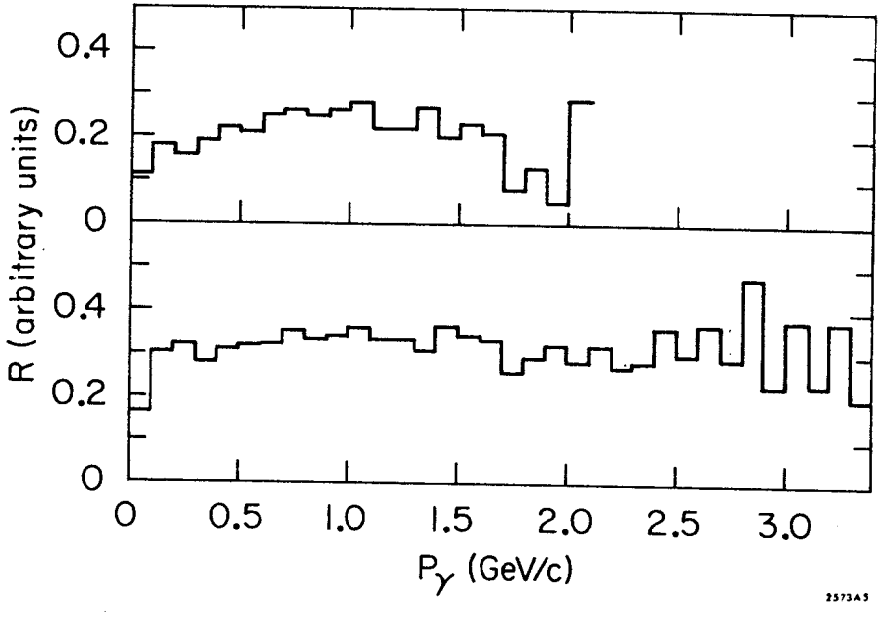

FIG. 11--Ratio R = (number of gammas at p_γ in data)/(number of gammas at p_γ in Monte Carlo).

approximations are necessary, such as found in Rossi.[79] Using this figure and our measured gamma spectrum, we estimate the conversion probability to be 55%. A direct experimental measurement has recently been published,[80] from which we read off the maximum probability of detecting a charged particle at a given depth to be 51±3% for our converter. Having measured ~46%, we attribute the difference to TOF cuts eliminating real gammas, and a small software inefficiency for locating showers in the data.

C. Normalization

Since the experimental problems associated with finding and reconstructing the decay modes $K_L \to \pi\pi\gamma$ and $K_L \to \pi\pi\pi^o$ are quite similar, our primary measurement consists of the ratio R:

$$R = \frac{\Gamma(K_L^o \to \pi^+\pi^-\gamma)}{\Gamma(K_L^o \to \pi^+\pi^-\pi^o)}$$

In this manner the uncertainties that are difficult to duplicate in Monte Carlo (such as the probability of finding showers and the TOF precision) tend to cancel, provided that both sets of data are treated similarly. In fact, since R is proportional to the probability of converting and detecting one gamma from $\pi\pi\gamma$ decay, over the probability of converting and detecting one or two gammas from $\pi\pi\pi^o$ decay, the uncertainty in the branching ratio is insensitive to errors in the conversion efficiency, in fact $\left(\frac{\delta R}{R} \sim \frac{1}{8}\frac{\delta X}{X}\right)$.

We consistently require that events possess two charged tracks having a common vertex within the fiducial region, plus one or more showers. For purposes of normalization, we select $K_{\pi 3}$ events by demanding

1) $-0.002 < p_0'^2 < 0.010\ (\mathrm{GeV/c})^2$
2) one or two gammas

3) neither charged track be identified as an electron or a muon
4) $\cos\theta_{\gamma C} < 0.9996$, where $\theta_{\gamma C}$ is the angle in the laboratory between the direction of the γ ray and either charged track at the decay vertex.

The final cut serves to remove $K_{\ell 3}$ background in which the gamma is radiated by the lepton in passing through the front chambers or hodoscope bank. Several other minor cuts are imposed: $p_{\pi^o}^{\perp} < p_{\pi^o}^{*}$, where $p_{\pi^o}^{*}$ is the π^o c.m. momentum; $m_{\pi\pi} < m_K - m_{\pi^o}$, $|T_+ - T_-| < 1.5$ nsec, and $\left|T_\gamma - \left(\frac{T_+ + T_-}{2}\right)\right| < 1.0\ (2.0)$ for rear (front) gammas. Less than 1% of the 165K surviving events are due to leptonic contamination, however, losses of pions which have simulated electrons or muons amounts to 10%. Of this, pion decays in flight are duplicated in the Monte Carlo (approximately 4%) as well as showers accidently overlapping tracks, causing an electron misidentification (a further 1-2%). Thus, roughly 5% of the 3π data is lost, introducing a small bias into the normalization. A negligible bias is also introduced by including low momentum gammas for which the conversion efficiency is not determined. (Less than 1% have $p_\gamma < 150$ MeV/c.)

The acceptance is determined by comparing the number of Monte Carlo events which survive the above requirements with the number generated, making use of the proper gamma conversion efficiency. We employ the recently determined[77] matrix element for $K_{\pi 3}$:

$$|M|^2 \sim 1 - 5.2\,(Q/M_k)Y + 4.64\,(Q/M_k)^2 Y^2$$

where

$$Y = 3T_{\pi^o}/Q - 1 \quad ,$$

and the $K_{3\pi}$ branching ratio

$$\Gamma(K_L^o \to \pi^+\pi^-\pi^o)/\Gamma(K_L^o \to \text{all}) = 0.126 \quad .$$

The number of kaons decaying is found to be 31.8×10^6. Using completely reconstructed 3π events having two γ's, and making further kinematic requirements to completely eliminate the $K_{\ell 3}$ contamination provides a semi-independent verification which proves to be consistent with the ≥ 1 gamma sample actually employed.

V. KINEMATICAL ANALYSIS

A. The Decay $K_L^o \to \pi\pi\gamma$

To extract the $\pi\pi\gamma$ signal implies the isolation of a maximum of several hundred events (at the previous upper limit for the rate) from a sample containing hundreds of thousands of candidates. The knowledge of the gamma direction provides a two-constraint fit, without relying directly on the TOF for the K momentum.

Candidates for $\pi\pi\gamma$ decay are selected similarly to the 3π normalization sample:

1. $p_0'^2 < -0.014$ to eliminate the bulk of the $K_{\pi 3}$ triggers
2. one and only one gamma
3. neither charged track is identified as an electron or muon
4. $\cos\theta_{\gamma C} < 0.9996$ to eliminate leptonics with bremsstrahlung.

Several other minor kinematical cuts are made: ($m_{\pi\pi} < m_K$; $p_\gamma^\perp < p_\gamma^*$) where p_γ^* is the c.m. momentum of the γ, as well as a timing consistency check on the charged tracks and gamma: ($|T_+ - T_-| < 1.5$ nsec and $\left|T_\gamma - \frac{(T_+ + T_-)}{2}\right| < 1.0$ (2.0) for a rear (front) gamma). The remaining background is primarily $K_{\ell 3}$ (negative $p_0'^2$) having a random gamma in time with the charged tracks. The contribution from $K_{\pi 3}$ is quite small, having been eliminated by the $p_0'^2$ cut. The magnitudes and distributions of these are discussed in the following sections.

Two methods were used to identify $\pi\pi\gamma$ events: The first compared the predicted direction of the γ-ray with its measured direction, and the second compared $m_{\pi\pi\gamma}$ to m_K. At the outset, we calculated the gamma momentum from the conservation of transverse momentum and rejected events with $p_\gamma < 150$ MeV/c, since we had no accurate knowledge of the conversion

efficiency below this energy. In the first method, we calculated ψ, the angle between the measured and predicted γ-ray direction using $\vec{p}_{\pi^+}$, $\vec{p}_{\pi^-}$ and the K_L^o direction as shown in Fig. 12. Two solutions for the laboratory gamma direction arise due to a quadratic ambiguity, corresponding to forward and backward emission in the K_L center of mass system. The solution which gives the better agreement with the measured direction was chosen, which specifies an associated kaon momentum. The TOF associated with the kaon momentum is then compared to the measured time, and we demand $|TOF_{measured} - TOF_{fit}| \leq 0.7$ nsec. In addition, we learn from a consideration of the second technique (mass method) that the angle between the γ-ray and kaon, $\theta_{\gamma K}$, can have an important effect on the mass resolution, and in fact requires a cut (discussed further in the next section). The resolution of the reconstruction of cos ψ is well-behaved as $\theta_{\gamma K} \rightarrow 0$; however the background shows a slight enhancement, therefore a requirement that $\theta^2_{\gamma K} > 0.001$ is imposed. After this procedure, 106 front shower and 786 rear shower events remain. The values obtained from the data are plotted in Fig. 14 for cos $\psi > 0.9968$.

If our expectation that the background comes predominantly from random gammas is correct, then the background should be flat in cos ψ, i.e., if the gamma is predicted to hit at a point (x,y) on the lead sheet, and the randoms are uniformly distributed in the plane, then

the number dN of randoms between r and r+dr $= 2\pi r\, dr$

$\sin\psi = \frac{r}{\bar{Z}} \sim \psi$ where $\bar{Z}$ is the average ΔZ of the flight path of a gamma ray

$dr = \bar{Z}\, d\psi$

$dN = 2\pi\bar{Z}^2\, \psi\, d\psi = 2\pi\bar{Z}^2 \sin\psi\, d\psi$

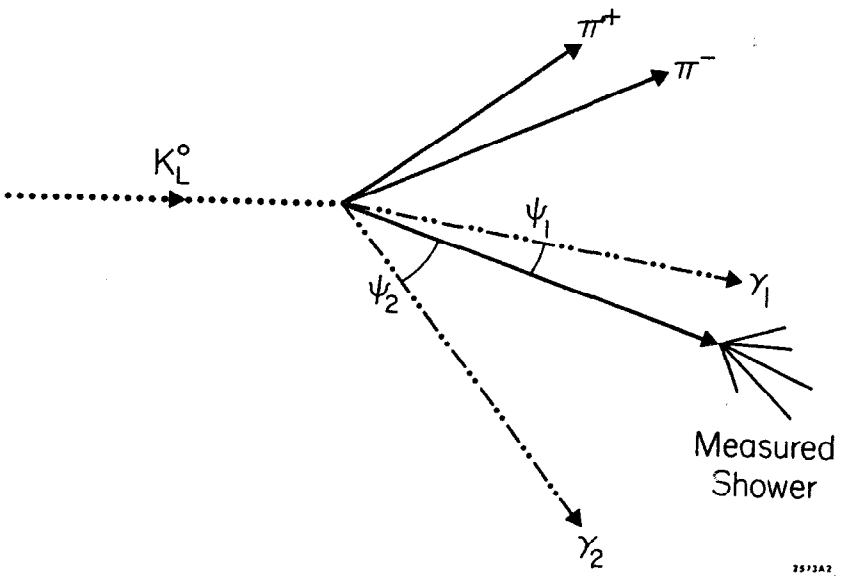

FIG. 12--Reconstruction geometry for cos ψ in $K_L^o \rightarrow \pi\pi\gamma$ decay.

$$\frac{dN}{d(\cos\psi)} = 2\pi\bar{Z}^2$$

The second method consisted of reconstructing the mass of the $\pi\pi\gamma$ system. First, the candidates were required to be consistent with the conservation of transverse momentum by applying $\Delta\phi$ cuts of 450 (150) mrads for the front (rear) showers, where $\Delta\phi$ is the difference between the predicted and measured γ angle in the plane perpendicular to the K_L^o direction. Figure 13 shows the geometry for this reconstruction.

The gamma momentum is then computed using the charged transverse momentum and the gamma direction: $|P_\gamma| = |P_\mp^\perp|/\sin\theta_{\gamma K}$. A fitted TOF corresponding to the momentum of the kaon as computed from all the outgoing particles is then compared to the measured momentum, and again we require $|TOF_{fit} - TOF_{meas}| < 0.7$ nsec. The conservation of transverse direction requirement reduced the 1074 candidates to 79, whose invariant mass is plotted in Figure 14c.

The mass of the $\pi\pi\gamma$ system is equal to:

$$M^2_{\pi\pi\gamma} = M^2_{\pi\pi} + 2P^2_{\pi\pi}\left(\frac{\sin\theta_{\pm K}}{\sin\theta_{\gamma K}}\right)\left\{\left[1 + \frac{M^2_{\pi\pi}}{P^2_{\pi\pi}}\right]^{\frac{1}{2}} - \cos\theta_{\pm\gamma}\right\}$$

where $M_{\pi\pi}$ ≡ invariant mass of dipion system

$P_{\pi\pi}$ ≡ magnitude of dipion momentum

$\theta_{\pm K}$ ≡ angle between $\pi^+\pi^-$ system and kaon

$\theta_{\pm\gamma}$ ≡ angle between $\pi^+\pi^-$ system and gamma

$\theta_{\gamma K}$ ≡ angle between gamma and kaon

which is approximately equal to

$$M^2_{\pi\pi\gamma} \approx M^2_{\pi\pi} + \frac{P^2_{\pi\pi}\,\theta^2_{\pm\gamma}\,\theta_{\pm K}}{\theta_{\gamma K}}$$

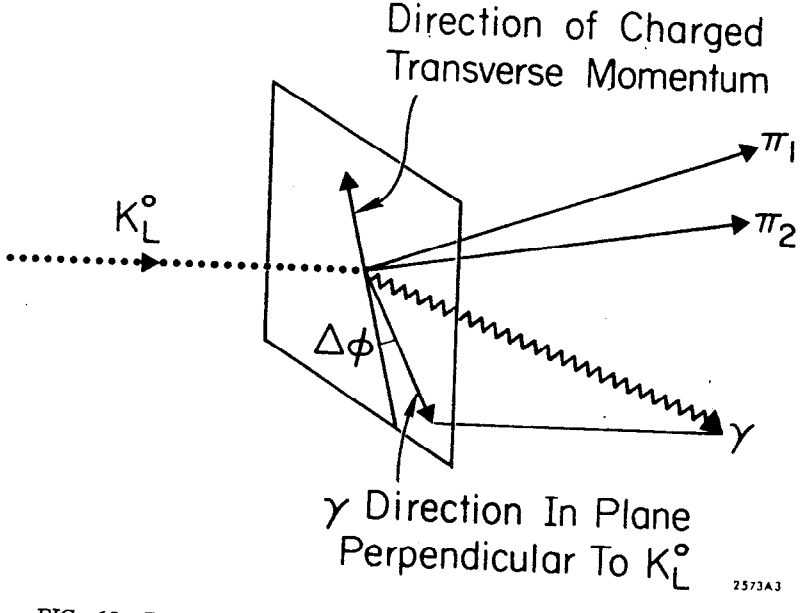

FIG. 13--Reconstruction geometry for $m_{\pi\pi\gamma}$ in $K_L^o \to \pi\pi\gamma$ decay.

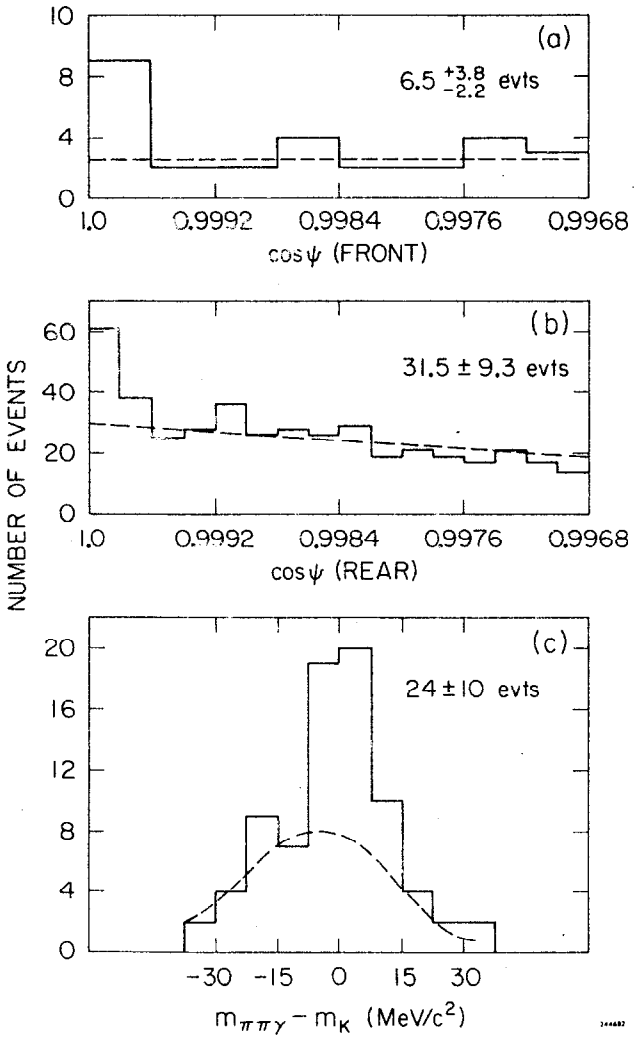

FIG. 14--(a) cos ψ, the angle between the measured and predicted γ-ray directions for $\pi\pi\gamma$ candidates with a front γ shower. (b) cos ψ for $\pi\pi\gamma$ candidates with a rear γ shower. (c) $m_{\pi\pi\gamma} - m_{K^0}$. The backgrounds discussed in the text are indicated by dashed lines.

Note that the mass of the $\pi\pi\gamma$ system is not well-defined as $\theta_{\gamma K}$ goes to zero. Therefore, as in the "cos ψ method", we impose the requirement that $\theta^2_{\gamma K} > 0.001$ or that $\theta_{\gamma K} > 33$ mrad.

We conclude that both methods yield significant evidence for the presence of $\pi\pi\gamma$ signal; however we must still investigate whether any of the potential sources of background could peak at m_K or cos $\phi = 1.00$. We note that different regions of p'^2_0 imply different sources of background, as shown in Fig. 15.

The decay $K^o_L \to \pi^+\pi^-\pi^o$ would naturally be expected to be the prime contributor since there are two pions and two gammas in the final state, of which we may detect only one. However, $p'^2_0 > 0$ is an extremely effective signature for the decay, and we can check that no enhancement at $p'^2_0 \sim -0.014$ still persists after cuts. In addition, we attempt to learn the detailed shape of the p'^2_0 distribution for $K_{\pi 3}$ in the negative region by selecting events on the DST having two gammas but passing all the $\pi\pi\gamma$ cuts except for p'^2_0 and the p^T_γ cut which is closely related. After making a correction for leptonic feedthrough into the $K_{\pi 3}$ sample via random gammas, we can learn the fraction of $K_{\pi 3}$ within the $\pi\pi\gamma$ region which appear as candidates for the cos ψ method. Knowing this fraction and the total number of $K_{\pi 3}$ decays enables a calculation of the number persisting onto the cos ψ plot. We find this contamination to be less than 5% (or less than 50 events). Furthermore, Monte Carlo simulations of $K_{\pi 3}$ decays show no evidence of peaking at the signal region, even if pathologically large scatters are introduced into the kaon's or pion's direction. Certainly this source cannot account for the observed peaks in both the cos ψ and mass plots, since an additional 10^{-2} reduction due to the $\Delta\phi$ requirement

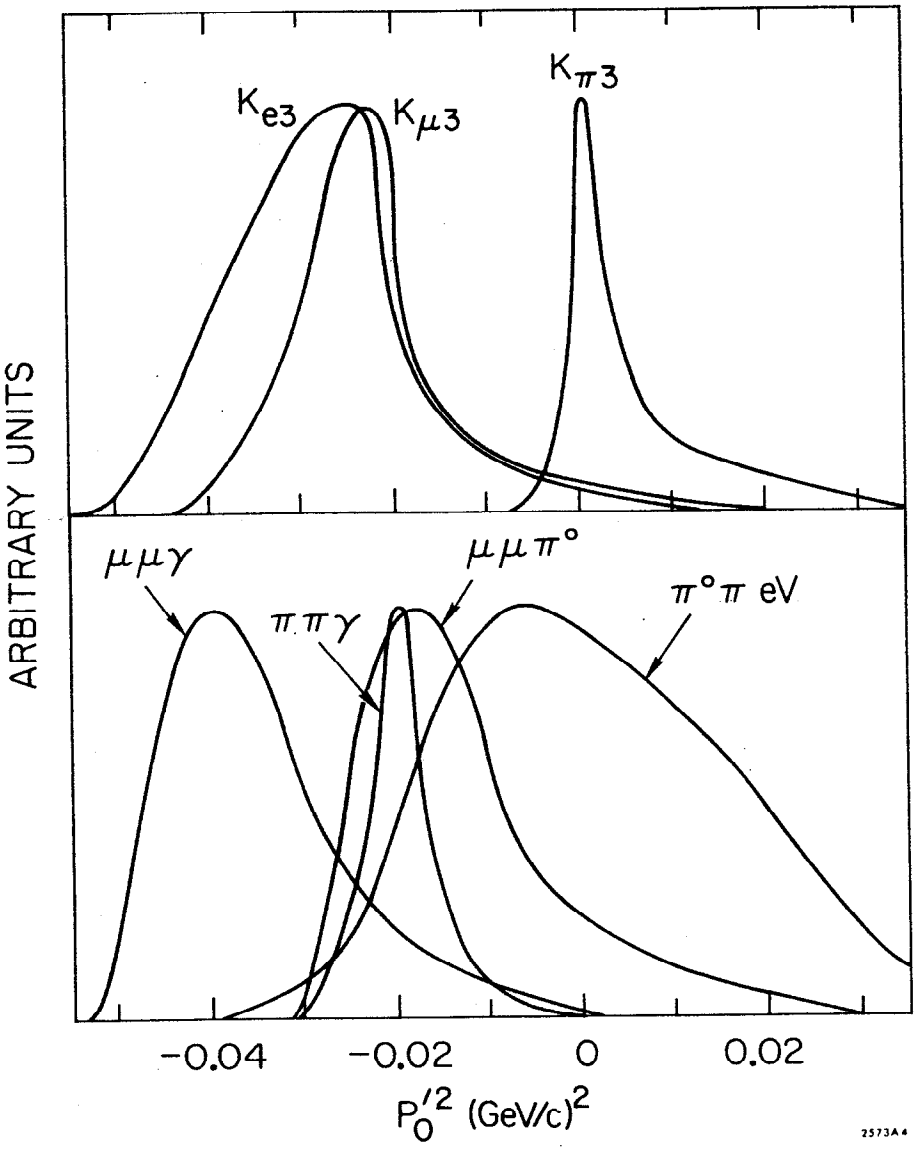

FIG. 15--Distributions of $p_0'^2$ for various K_L^o decays.

leaves too few potential $K_{\pi 3}$ on the mass plot which, furthermore, have no peaking characteristics.

The decay $K_L^o \rightarrow \pi^{\pm}$ ($\mu^{\mp}$ or $e^{\mp}$, unidentified) ν plus an accidental in-time shower can contribute to the $\pi\pi\gamma$ signal, since $p_0'^2$ for this decay overlaps the $\pi\pi\gamma$ region. We simulate this decay using the Monte Carlo and inserting a "random" gamma. We also select events on the DST wherein the lepton was identified and check the distributions on the final plots. Finally, we assume (to a good approximation) that all the events on the cos ψ plot are $K_{\ell 3}$ with a random gamma except for the signal. These may then be studied by reshuffling the gammas, so that the photon (which has already passed all its timing and quality requirements) is reassigned to another event. To the extent that the signal events constitute a small fraction of the candidates, this technique has a built-in normalization, as well as the assurance that these photons have as many real characteristics as possible. All of these techniques share the common property that in no case is there a peaking in the signal region, so that even though these events form the bulk of the DST, they cannot account for the signal we observe.

Figure 16 shows the distributions obtained for the Monte Carlo simulations of K_{e3} and $K_{\mu 3}$, as well as the events on the DST passing $\pi\pi\gamma$ cuts but with the lepton identified. The process of reassigning gammas to another event reproduces the shape of the distribution outside the signal so well that we employ several such reshufflings to obtain a smooth fit to the random gamma background. The dashed lines shown in Fig. 14 are the average results, to which we have fitted a 4th order polynomial on the mass plot, a 0th order polynomial to cos ψ_F, and a second order fit to the cos ψ_R events. The dashed lines appear on Fig. 14 as the contribution from background.

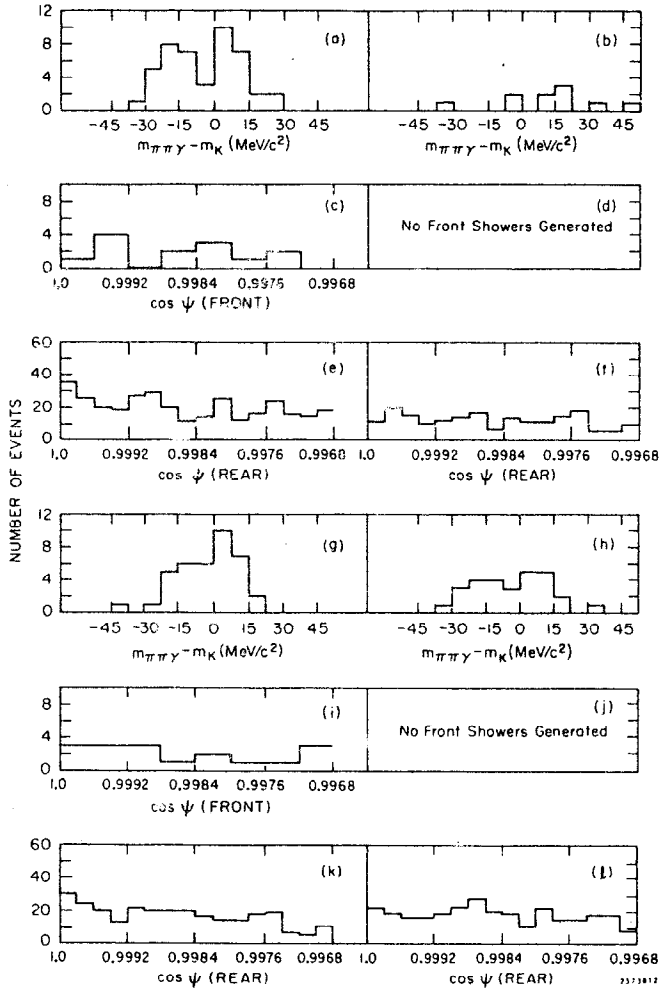

FIG. 16--Background estimates for $K_L^o \to \pi\pi\gamma$. (a), (c), (e) are events from the $\pi\pi\gamma$ data summary tape having an identified electron. (b), (d), (f) are Monte Carlo simulations of K_{e3} decay analyzed as $\pi\pi\gamma$. (g), (i), (k) are events from the $\pi\pi\gamma$ data summary tape having an identified muon. (h), (j), (ℓ) are Monte Carlo simulations of $K_{\mu 3}$ decay analyzed as $\pi\pi\gamma$. The Monte Carlo simulations are not normalized.

We note that the background subtraction does not depend strongly on which method we use; at this level, an eyeball fit or a fit to the tails of the distribution would serve adequately; however, we choose to employ the random gamma technique since it is well understood and appears to explain the background very well.

The three distributions of Fig. 14, when combined with the Monte Carlo acceptance calculations (for which the matrix elements are discussed in the following section) and the $K_{\pi 3}$ normalization provide three correlated determinations of the $K_L^o \to \pi\pi\gamma$ branching ratio. In all cases, we increase the systematic uncertainty on the background, since we have not included explicit subtractions for $K_{\pi 3}$ or $K_{e3,\gamma}$, and then fold in the systematic uncertainty in the peak. In Fig. 14c, we accept events within ±7.5 MeV of m_K, from which we obtain (39 - 15) ± 6.2 (statistical) ± 8 (background) = 24 ± 10 events. We accept events with $\cos\psi_F > .9996$, from which we have (9 - 2.5) ± 3.7 (statistical) ± 1 (background) = $6.5^{+3.8}_{-2.2}$ events and for $\cos\psi_R > .9998$ we have (61 - 29.5) ± 7.8 (statistical) ± 5 (background) or 31.5 ± 9.3 events. These then yield $R \equiv \Gamma(K_L^o = \pi^+\pi^-\gamma)/\Gamma(K_L^o \to \pi^+\pi^-\pi^o)$:

$$\underline{\text{Mass Plot}} \to R = (3.8 \pm 1.6) \times 10^{-4}$$

$$\underline{\cos\psi_F} \to R = (5.3 \pm \tfrac{3.1}{1.8}) \times 10^{-4}$$

$$\underline{\cos\psi_R} \to R = (5.8 \pm 1.6) \times 10^{-4}$$

Weighting these results by $1/\sigma^2$ gives an overall average

$$R = (4.9 \pm 1.7) \times 10^{-4}$$

Using $\Gamma(K_L^o - \pi^+\pi^-\pi^o/\Gamma(K_L^o \to \text{all}) = .126$, this corresponds to

$$\Gamma(K_L^o \to \pi^+\pi^-\gamma)/\Gamma(K_L^o \to \text{all}) = (6.2 \pm 2.1) \times 10^{-5}$$

1. Comparison with Predicted Branching Ratios

Our measured branching ratio is consistent with only two of the calculations previously discussed. These are a 1967 current algebra calculation by C. S. Lai and B. L. Young,[13] and a zero-free parameter baryon loop model by R. Rockmore and T. F. Wong[31] in 1973.

Lai and Young predict $\Gamma(K_L^o \to \pi\pi\gamma, \text{ direct emission})/\Gamma(K_L^o \to 2\gamma) \simeq 0.14$; therefore, when the present value $\Gamma(K_L^o \to 2\gamma)/\Gamma(K_L^o \to \text{all}) = 4.9 \times 10^{-4}$ is used, we expect that $\Gamma(K_L^o \to \pi\pi\gamma)/\Gamma(K_L^o \to \text{all}) \simeq 6.8 \times 10^{-5}$.

Rockmore and Wong approach the problem via a modified fermion loop model which has no adjustable parameters. Their unrenormalized result is $r = 7.51 \times 10^{-5}$, which is in good agreement with our measurement.

These values are to be compared with the predictions for inner bremsstrahlung (IB): Lai and Young have computed that $r = \Gamma(K_L^o \to \pi\pi\gamma, \text{ IB})/\Gamma(K_L^o \to \pi^+\pi^-) = 1.1 \times 10^{-2}$ for $E_\gamma^* > 10$ MeV and 2.6×10^{-3} for $E_\gamma^* > 50$ MeV.

Therefore we expect

$$r = 1.73 \times 10^{-5} \text{ for } E_\gamma^* > 10 \text{ MeV}$$

$$r = 0.41 \times 10^{-5} \text{ for } E_\gamma^* > 50 \text{ MeV}$$

Both the measured rate and observed gamma spectrum imply that inner bremsstrahlung does not dominate this decay.

Finally, Alles, Gaillard and Pati obtain[43] the maximum suppression to the $K_L \to \mu\mu$ rate due to the $\pi\pi\gamma$ intermediate state is 2 - 4% using the previous best upper limit on $K_L \to \pi\pi\gamma$. Their expression for the suppression R to this rate includes a factor

$$R = \left[\frac{\alpha}{6\pi} \frac{\Gamma(K_L \to \pi\pi\gamma)}{\Gamma(K_L \to 2\gamma)}\right]^{\frac{1}{2}}$$

and they have used

$$\Gamma(K_L \to \pi\pi\gamma)/\Gamma(K_L \to \text{all}) = 4 \times 10^{-4}$$

$$\Gamma(K_L \to 2\gamma)/\Gamma(K_L \to \text{all}) = 5 \times 10^{-4}$$

Using the current values

$$\Gamma(K_L \to \pi\pi\gamma)/\Gamma(K_L \to \text{all}) = 6.2 \times 10^{-5}$$

$$\Gamma(K_L \to 2\gamma)/\Gamma(K_L \to \text{all}) = 4.9 \times 10^{-4}$$

the ratio $\left[\frac{\Gamma(K_L \to \pi\pi\gamma)}{\Gamma(K_L \to 2\gamma)}\right]^{\frac{1}{2}}$ goes from 0.89 to 0.36; therefore, the maximum decrease in the $K_L \to \mu\mu$ unitarity limit is 1.6%.

2. Dalitz Plot Distribution for $K_L^o \to \pi\pi\gamma$

As mentioned in the discussion of the theoretical aspects of $K_L \to \pi\pi\gamma$, the decay can proceed either through CP violating $K_L \to \pi\pi$ + a photon from inner bremsstrahlung (IB), or via a CP conserving direct emission (DE) process. Since the bremsstrahlung process should populate the low-gamma momentum region in the center of mass, it would be easily distinguishable from the direct process which tends to maximize the gamma momentum. We display in Fig. 17 an unusual appearing Dalitz Plot which is folded about the gamma energy axis, since the small number of events can best be interpreted when combined.

We choose to plot those events lying within ±7.5 MeV of m_K in Fig. 14c corresponding to a signal-to-noise ratio of roughly 3:2. This distribution does not depend on any Monte Carlo acceptances; it is simply a histogram of the observed events. Before we can attribute a particular matrix element to this spectrum we must first know the appearance of the different choices on the Dalitz plot after the acceptance of the apparatus has been folded in. Finally, the shape and magnitude of the background can be estimated and

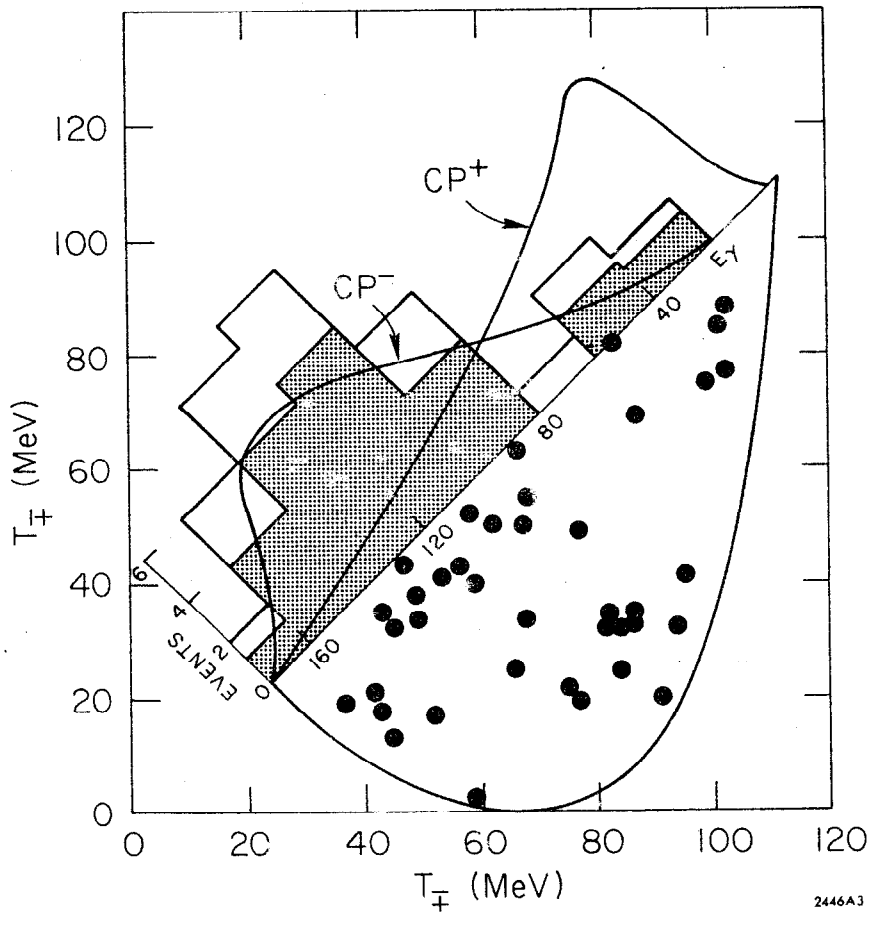

FIG. 17--Dalitz plot (folded about the γ energy axis) and projected γ-ray energy spectrum. The shaded portion is the difference between the observed distribution and the expected background. The smooth curves show the predicted spectra including experimental acceptance for $L_{\pi\pi}=1$, CP conserving (-) and violating (+) matrix elements.

removed from the observed distribution. We can then compare the shape of the signal after subtraction with the Monte Carlo shapes corresponding to various possible quantum numbers of the final states.

To generate $\pi\pi\gamma$ decay in the Monte Carlo, we need only consider states having $L_{\pi\pi} = 1$ or 2, since the available energy (215 MeV) makes higher L unlikely.

Since it appears most likely that the emission is E1 or M1 (the lowest possible angular momentum state), we generate both these possibilities using the matrix elements as written in Beder.[12] The resulting gamma spectra with the apparatus' acceptance included appear in Fig. 17 as smooth curves. Qualitatively, the $L_{\pi\pi} = 1$ CP (-) matrix element due to magnetic dipole emission resembles a phase space distribution. The bremsstrahlung distribution peaks distinctively at low p_γ, with the cutoff due to the requirement that $p_\gamma >$ 150 MeV in the lab system.

If the decay proceeds via the CP violating mode $K_L \rightarrow \pi\pi$ followed by inner bremsstrahlung, one expects a branching ratio of roughly 1×10^{-5} (for $E^*_\gamma > 20$ MeV) as well as the bremsstrahlung energy distribution. The accepted γ spectrum produced by this process is such that no cut on E^*_γ was necessary to obtain the branching ratio. Thus we observe that the crude Dalitz plot distribution of these events (as well as the measured branching ratio) is consistent with a CP conserving magnetic dipole transition dominating the decay. Therefore, those who would search for CP violating effects in the strong or electromagnetic interactions in the K system must wait until the experiments reach yet another level of sensitivity.

B. The Decays $K_L^o \to \mu\mu\gamma$ and $\mu\mu\pi^o$

The observation of two muons penetrating the lead wall provides a rather powerful signature which is not easily duplicated by background processes. The additional presence of one or more valid photon showers then implies an extremely clean sample in which to test the hypothesis $K_L^o \to \mu^+\mu^-\gamma$ or $\mu^+\mu^-\pi^o$. This spectrometer is well adapted to resolve these events, making use of the two-stage muon filter and excellent shower conversion point resolution; however, the expected rates are very low ($\sim 10^{-7}$) and the geometric acceptance small. Thus it is not surprising that, in some thirty million K decays, we observe no events.

To begin the reconstruction, we select those events containing two identified muons which verticize and have one or more photon showers. One shower is sufficient to overdetermine the decay $K_L \to \mu^+\mu^-\gamma$; however, two are required for the decay $K_L \to \mu^+\mu^-\pi^o$. If only a single photon is observed in the latter mode, an "OC situation" exists; however, the necessity of detecting both photons from the π^o decay reduces the sensitivity by roughly an order of magnitude relative to the $\mu\mu\gamma$ decay. Both decay modes have the same requirements on the goodness of vertex, track fitting, and shower quality.

Events having only one shower are tested as $\mu\mu\gamma$ candidates. Two minor kinematical requirements have been imposed:

(1) $m_{\mu\mu} < m_K$ $\quad m_{\mu\mu}$ is the invariant mass of the 2μ system

(2) $p_\gamma^T < p_\gamma^*$ $\quad p_\gamma^T$ is the transverse momentum of the γ-ray

p_γ^* is the momentum of the gamma in the kaon rest frame

The event topology is then required to be roughly consistent with the conservation of transverse momentum; i.e., the direction of the gamma must lie

opposite the charged transverse momentum. We require $\Delta\phi$ be less than 450 (150) mrad for front (rear) showers, where $\Delta\phi$ (as in $\pi\pi\gamma$ decay) is the difference between the predicted and measured γ angle in the plane perpendicular to the K_L^o direction. Since we finish with no viable candidates, it is not necessary to impose cuts on p_γ or $\theta_{\gamma K}$ as it was in the $\pi\pi\gamma$ analysis. The above cuts reduce the 383 candidates to 43 survivors.

We reconstruct the mass of the $\mu\mu\gamma$ system, exactly as for $\pi\pi\gamma$, using p_μ^+, p_μ^-, and $p_\gamma = p_\pm^T/\sin\theta_{\gamma K}$, where $p_\pm^T$ is the sum of the charged transverse momentum and $\theta_{\gamma K}$ is the angle between the photon and the kaon.

A scatter plot of the mass of these events versus $p_0'^2$ (Fig. 18) demonstrates that we observe no candidates within ±10 MeV of m_K, and that our predominant source of background is $K_{\pi 3}$ decays (which have a positive $p_0'^2$) in which the pions have decayed or penetrated. We conclude that there is no evidence for the decay $K_L^o \to \mu\mu\gamma$.

The other expected background is $K_{\mu 3}$ decay having one pion tagged as a muon, with an accidental shower in time with the event.

As in the case of the $\pi\pi\gamma$ analysis, we can learn the acceptance of $K_{\pi 3}$ by including the pion decays in flight in the Monte Carlo, and by artificially allowing the pions to punch through. Even after these pions are assigned muon masses, the population on the mass vs $p_0'^2$ plot remains restricted to low value for the mass (peaking around 350 MeV), and positive $p_0'^2$. Thus we expect no candidates from $K_{\pi 3}$ to be present in the signal region, and the distribution we observe is consistent with the predicted shape and number.

The background from $K_{\mu 3}$ decays having an accidental gamma is somewhat harder to rule out. $p_0'^2$ for this leptonic decay overlaps the $\mu\mu\gamma$ region, and the accidental photon can occur at virtually any point on the lead sheet; so

that it will sometimes occur at exactly the right point to simulate the necessary gamma momentum. We generate $K_{\mu 3}$ decays and insert a shower conversion point distributed randomly across the converter in such a way as to crudely match the observed distributions of showers. Both pion decays in flight and punch-throughs are taken into account, and we expect a distribution of events having the characteristic $K_{\mu 3}$ shape for $p_0'^2$ with the corresponding $m_{\mu\mu\gamma}$ rather broadly scattered. We note that candidates having negative $p_0'^2$ are distributed in this manner; therefore, we can understand the observed leptonic background and it is fortunate that no events lie within ±10 MeV of m_K.

The Monte Carlo generation of the decay $K_L^o \to \mu\mu\gamma$ employed the matrix elements given in Sehgal.[51] The rate for the process depends on a knowledge of the $K_2^o \to \gamma\gamma$ vertex when one of the photons is off the mass shell. The dependence of this vertex on t, the invariant (mass)^2 of the virtual photon is expressed using a form factor $F_2(t)$. In the limit when this form factor is constant, the differential decay rate for the Dalitz process is given by

$$\frac{d\Gamma(K_2^o \to \bar{\ell}\ell\gamma)/dt}{\Gamma(K_2 \to \gamma\gamma)} = \frac{2\alpha}{\pi}\left(1 - \frac{t}{m_k^2}\right)^3\left(1 + \frac{2m_\ell^2}{t}\right)\left(1 - \frac{4m_\ell^2}{t}\right)^{\frac{1}{2}}\frac{1}{t}$$

where m_k and m_ℓ are the kaon and lepton masses. If this form factor is not constant a significant deviation from the above may result. Sehgal displays this displacement graphically, and we employ a matrix element with a vector meson form factor included.

We have observed no events conforming to the hypothesis $K_L^o \to \mu\mu\gamma$; therefore we infer that the number of events in this experiment should follow a Poisson distribution. We quote an upper limit for the branching ratio

corresponding to the observation of 2.3 events at the 90% confidence level. This, together with the Monte Carlo acceptances mentioned above, yields a branching ratio $\Gamma(K_L^o \to \mu^+\mu^-\gamma)/\Gamma(K_L^o \to \pi^+\pi^-\pi^o) \leq 6.20 \times 10^{-5}$ and using $\Gamma(K_L^o \to \pi^+\pi^-\pi^o)/\Gamma(K_L^o \to \text{all}) = .126$ we obtain $\Gamma(K_L^o \to \mu^+\mu^-\gamma)/\Gamma(K_L^o \to \text{all}) \leq 7.81 \times 10^{-6}$ (90% C. L.).

This upper limit excludes the Alles and Pati model[53] which predicted a rate of $K_L \to \mu\mu\gamma$ greater than 6×10^{-4} arising from a light neutral boson decaying to μ pairs. In addition, a recent Russian experiment[81] has shown that $\Gamma(K_L^o \to e^+e^-\gamma)/\Gamma(K_L^o \to \text{all}) < 2.8 \times 10^{-5}$, which is about a factor of 50 lower than the Alles-Pati prediction. Unfortunately the more interesting predictions, and even the Dalitz pair rate, are more than an order of magnitude below this limit.

Both one and two shower events are tested as $K_L^o \to \mu^+\mu^-\pi^o$ candidates. The corresponding kinematical requirements are imposed:

$m_{\mu\mu} < m_K - m_{\pi^o}$

$p^*_{\pi^o} > 0$ $\quad$ $p^*_{\pi^o}$ is the momentum of the π^o in the K center of mass system

$p^T_{\pi^o} < p^*_{\pi^o}$ $\quad$ $p^T_{\pi^o}$ is the transverse momentum of the π^o in the laboratory.

These reduce 427 $\mu\mu$ candidates to 333 survivors, of which 35 have two showers. Sufficient constraints then exist to determine the direction of the π^o, which must lie in the plane containing the two gammas, and also in the plane containing the direction of the K_L^o and the charged transverse momentum. The π^o direction together with the opening angle of the 2γ system allows a computation of $m_{\mu\mu\pi^o}$. A scatter plot of $m_{\mu\mu\pi^o}$ versus $p_0'^2$ is shown in Fig. 18b. No requirements whatsoever have been made on the reconstructed mass of the 2γ system, which displays the origin of the remaining background. The

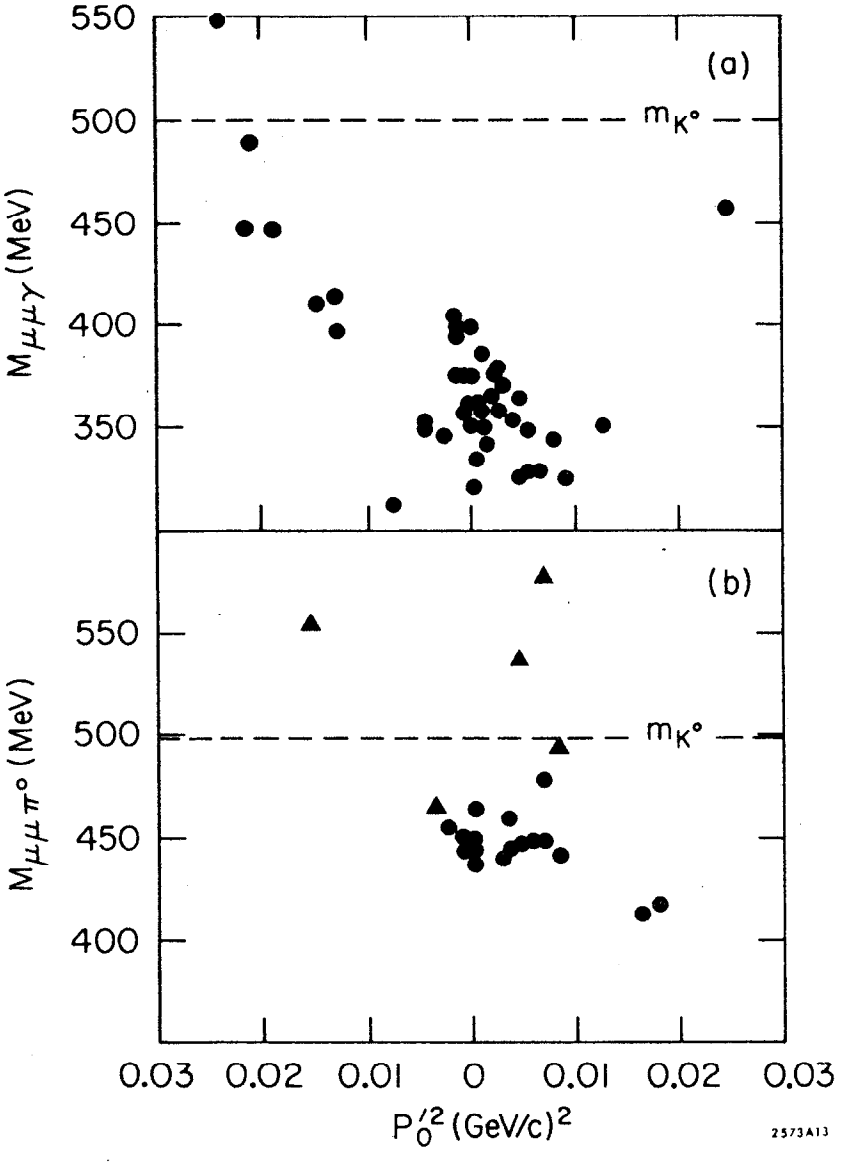

FIG. 18--Reconstructed mass of (a) $K_L^0 \rightarrow \mu\mu\gamma$, (b) $K_L^0 \rightarrow \mu\mu\pi^0$ events versus $p_0'^2$. Events plotted as triangles in (b) have $m_{2\gamma} > 500$ MeV/c^2.

events plotted as triangles have the 2γ mass (which should equal m_{π^0}) greater than 500 MeV. Including this as a kinematical requirement changes the acceptance by less than 2%. Virtually all the background has $p_0'^2 > 0.02$, and is therefore most likely due to $K_{\pi 3}$ decays. The portion which has $m_{2\gamma} \approx m_{\pi^0}$ is very likely due to both gammas originating in the π^0 decay, whereas the other most probably has one gamma from the pi-zero and one spurious gamma. This is corroborated by Monte Carlo simulations, and we determine that the peaking at $m_K = 450$ MeV is characteristic of $K_{\pi 3}$ decay with both photons detected. Since a spurious gamma can determine a completely non-physical two-gamma plane, it should come as no surprise that the total reconstructed mass of a system containing such a random process can vary over a wide range. Still others of the 35 remaining 2γ candidates have reconstructed $m_{\mu\mu\pi^0}$ off the plot shown in Fig. 18b.

Circumstances surrounding the measurement of the decay $K_L \rightarrow \mu\mu\pi^0$ are such that the mere detection of this decay would be a matter of some interest, independent of the details of the process itself. Various models are discussed in Singh and Wolfenstein,[56] as well as Okubo and Bace,[57] which give expressions for possible matrix elements; however, the Monte Carlo acceptance we will employ derives from a purely phase space distribution. The theoretical considerations involved in calculating this rate are sufficiently complex that for the present this represents an easily modified and model-independent approach.

Again, since we have observed no $K_L \rightarrow \mu\mu\pi^0$ events, we quote the branching ratio as less than or equal to that corresponding to the observation of 2.3 events at a 90% confidence level. These hypothetical 2.3 events together with the acceptance arising from a phase space distribution from the

Monte Carlo imply a branching ratio $\Gamma(K_L^o \to \mu\mu\pi^o)/\Gamma(K_L^o \to \text{all}) \leq 5.66 \times 10^{-5}$ where as before the normalization to $K_{\pi 3}$ is implied.

The only quantitive prediction for $K_L \to \mu\mu\pi^o$ to appear in the literature is from Okubo and Bace, who obtain a branching ratio $\sim 0.65 \times 10^{-6}$. This is certainly consistent with the measured upper limit.

By comparison, a recent paper by Gaillard and Lee[48] obtains a rate for $K_L \to ee\pi^o$ which is "strongly suppressed" relative to other decays having branching ratios as low as 10^{-13}. According to Okubo and Bace, the ratio of $\mu\mu\pi$ to $ee\pi$ is expected to be roughly 0.4, so that increasing the sensitivity by two orders of magnitude (or, alternatively, detecting the decay $K_L \to ee\pi^o$) would provide a discrimination between these two calculations.

C. The Decay $K_L^o \to \pi^o\pi^\pm e^\mp \nu$

The final state $\pi^o\pi^\pm e^\mp \nu$ is an extremely difficult channel to reconstruct, since the neutrino is not detected and the presence of a π^o must be inferred by observing its decay into photons. If one can obtain the direction of the π^o, then the gamma-gamma opening angle specifies the pion energy as well. The timing information establishes the momentum of the kaon, and we can compare the reconstructed neutrino mass m_ν to its known value.

We begin by selecting events in which the two charged tracks have been identified as a pion and an electron and require an additional two gamma showers. The π^o must lie between the gammas, and, since the π^o decay distribution is isotropic in its center of mass system, its direction will tend to bisect the 2γ opening angle in the laboratory system. We test the resolution of this assumption by comparing the reconstructed π^o momentum with the originally generated Monte Carlo value with the results shown in Fig. 19. In contrast to the other decay modes, we rely on the timing information directly to establish

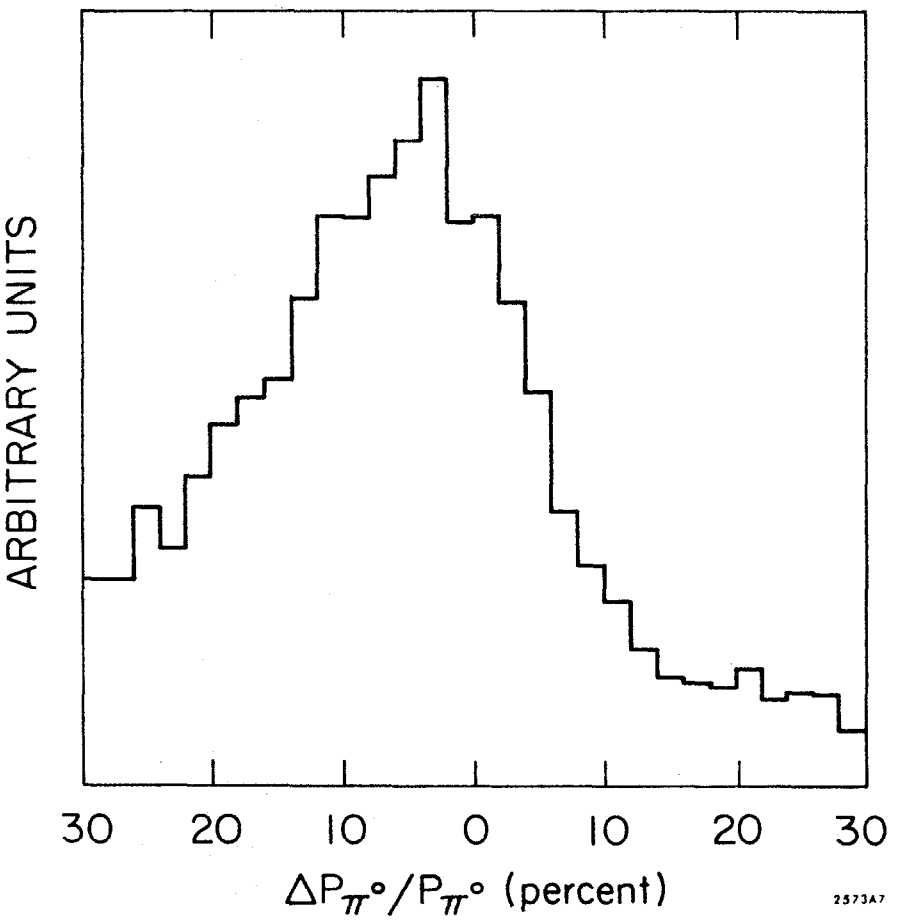

FIG. 19--Percentage error in π^o momentum in $K_L^o \to \pi^o\pi e\nu$ decay, assuming the π^o bisects the two gamma angle in the laboratory.

the K_L^o momentum. This is unavoidable, but unaesthetic for several reasons: First, the momentum resolution depends on the error made in the timing as $\Delta p/p = \gamma^2 \Delta T/T$, where $\gamma = E_k/m_k$. Second, the timing resolution is not well duplicated in the Monte Carlo and to this extent the Monte Carlo acceptance does not reflect the processes in the spectrometer.

Kinematical requirements are imposed on the decay:

(1) $P_0'^2 < -.005$ to reduce $K_{\pi 3}$ contamination

(2) $m_{\pi e} < m_k - m_{\pi o}$ to reduce $K_{\ell 3}$ contamination

(3) $\cos \Theta_{\gamma e} < 0.9996$ to reduce bremsstrahlung photons

$\cos \Theta_{\gamma\pi} < 0.9999$

(4) P_{π^o} requirements:

a) $P_{\pi^o}/P_K < 0.6$

b) $P_{\pi^o} < 6$ GeV/c

c) $p' < 2$ as defined below:

$$\vec{p}_k = \vec{p}_{\pi^o} + \vec{p}_{\pi e} + \vec{p}_\nu$$

$$p_{\pi^o}^2 = p_K^2 + p_{\pi e}^2 + p_\nu^2 - 2\,\vec{p}_k \cdot \vec{p}_{\pi e} - 2\vec{p}_K \cdot \vec{p}_\nu + 2\vec{p}_{\pi e} \cdot \vec{p}_\nu$$

$$= \left| p_K^2 + p_{\pi e}^2 - 2\vec{p}_K \cdot \vec{p}_{\pi e} \right| + \left| p_\nu^2 - 2\vec{p}_K \cdot \vec{p}_\nu\ 2\vec{p}_{\pi e} \cdot \vec{p}_\nu \right|$$

$$p'^2 \equiv p_{\pi^o}^2 \Big/ \left| p_K^2 + p_{\pi e}^2 - 2\vec{p}_K \cdot \vec{p}_{\pi e} \right| = 1 + \frac{\left| p_\nu^2 - 2\vec{p}_K \cdot \vec{p}_\nu + 2\vec{p}_{\pi e} \cdot \vec{p}_\nu \right|}{\left| p_K^2 + p_{\pi e}^2 - 2\vec{p}_K \cdot \vec{p}_{\pi e} \right|}$$

The acceptance for $\pi^o \pi e \nu$ events is very small, since the $p_0'^2$ cut passes only 43%, and the photon conversions reduce the sample by a factor of four. We plot $x \equiv \left(\frac{m_\nu}{m_{\pi^o}} \right)$, for which we expect 64% of the signal to lie within $|x| \leq 1.0$. In the data, we find the distribution shown in Fig. 20, which has 17 events

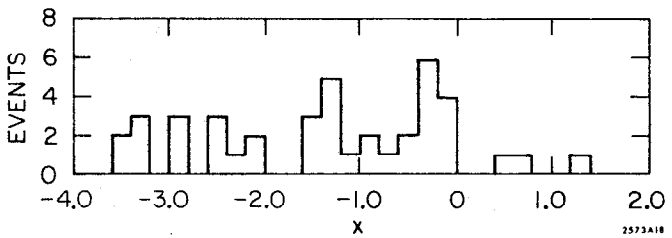

FIG. 20--Reconstructed neutrino mass^2 in $K_L^o \to \pi^o \pi e \nu$ decay. $x = (m_\nu/m_{\pi^o})^2$.

remaining. We expect several background processes to contribute: 1) $K_{\pi 3}$ decays in which a pion has been misidentified as an electron, and the two showers arise from a combination of real or accidental photons; 2) K_{e3} decays having two spurious showers. These sources are simulated, and we compute the expected number of events, using:

N_K = number of kaons decaying = 31.8×10^6

$BR_{e3,\pi 3}$ = branching ratio for K_{e3} and $K_{\pi 3}$ = .39 or .12

$P_e(e)$ = probability of electron identification = .55

P_c = probability of gamma conversion = .46

$P_\pi(e)$ = probability that a pion is identified as an electron = .03

$P_\gamma(a)$ = probability of having an accidental gamma with the event = .026

$P_\gamma(b)$ = probability that a gamma is radiated by the electron = .003

ϵ = kinematical acceptance for each mode = $10^{-3} - 10^{-5}$

We expect

$$N_1\ (K_{e3},\ 2 \text{ acc. } \gamma s) = N_K * BR_{e3} * P_e(e) * P_\gamma^2(a) * \epsilon = 6.65$$

$$N_2\ (K_{e3},\ 1 \text{ real } \gamma,\ 1 \text{ brem. } \gamma) = 0.11 * N_1 = 0.7$$

$$N_3\ (K_{\pi 3},\ 2 \text{ real } \gamma s \text{ from } \pi^o) = N_K * BR_{\pi 3} * P_c^2 * 2P_\pi(e) * \epsilon = 2.04$$

$$N_4\ (K_{\pi 3},\ 1 \text{ real } \gamma,\ 1 \text{ acc. } \gamma) = N_K * BR_{\pi 3} * P_c * P_\gamma(a) * 2P_\pi(e) * \epsilon = .29$$

$$N_5(K_{\pi 3},\ 2 \text{ acc. } \gamma s) = N_K * BR_{\pi 3} * P_\gamma^2(a) * 2P_\pi(e) * \epsilon = \text{negligible}$$

$$N_{BKGD} = 9 \pm 3.3$$

where systematic effects have been included in this uncertainty. We subtract the expected background from the observed distribution to obtain the number of candidates:

$$N(\pi^o \pi e \nu) = 17 \pm \sqrt{17} - 9 \pm 3.3 = 8 \pm 5.2$$

The number of events corresponding to an upper limit at the 90% confidence level is

$$N(\pi^o \pi e \nu) \leq 8 + 2.3 * 5.2 \simeq 20$$

and the corresponding limit on the branching ratio is

$$\Gamma(K_L^o \rightarrow \pi^o \pi^\pm e^\mp \nu)/\Gamma(K_L^o \rightarrow \text{all}) \leq 2.2 \times 10^{-3} \text{ at } 90\% \text{ C.L.}$$

with systematic effects included in the standard deviation.

Due to the extreme contortions necessary to eliminate backgrounds in this experiment, the remaining sensitivity is quite insufficient to attain even the relatively modest levels needed to discriminate between the Okubo and Bace model and the current algebra calculation.

D. <u>The Decay $K_L^o \rightarrow \pi^+ \pi^- e^+ e^-$</u>

The decay $K_L^o \rightarrow \pi^+ \pi^- e^+ e^-$ requires a somewhat different treatment than the other decays in that four charged tracks originate at the decay vertex. We do not require the identification of the electrons since the efficiency would then be reduced by the square of the electron conversion probability; however, this immediately leads to ambiguities in the particle masses. Experimentally, the data sample is very clean and the principal background is expected to be $K_{\pi 3}$ decays with the π^o undergoing a subsequent Dalitz decay $\pi^o \rightarrow e^+ e^- \gamma$, or an interaction of the beam with the material in the spectrometer.

The additional tracks emanating from a single vertex required a reprocessing of PASS 2, which had originally been organized to accept only "two-prong" vertexes. For this decay, we accept only four-prong vertexes; however, sufficient constraints are available even if one of these prongs does not pass through the magnet. Two data samples are generated: one having all four segments matched through the magnet to make four tracks (4T), the other having three full tracks with an extra front track segment (3T + F). As in the other

decays, stringent requirements are made on the goodness of the vertex and the quality of the match between the front and rear track segments with 8D4. Several additional requirements are imposed on the data: (1) the event satisfies a 2T·3A trigger; (2) the event possesses proper charged combinations (++-- for 4T; ++- or --+ for 3T+F); (3) no track is identified as a muon; (4) the opening angle between every oppositely charged pair must be such that $\cos\theta_{\pm} < .9999$; (5) the separations in X and Y must be greater than 0.5 cm at the first plane of the wire chambers. The first of these eliminates a large fraction of the candidates which cannot be duplicated by the Monte Carlo. The charge combination cut will pass both signal and $K_{\pi 3}$ background, but would reject a subset of accidental vertexes. The final two cuts are intended to eliminate events in which two charged tracks coalesce in the chambers. These events must be discarded since this effect is not reproduced in the Monte Carlo where each spark is unique down to the spacing of a single wire.

The kinematic reconstruction depends primarily on the conservation of momentum; in that way we avoid making assumptions about the masses of the particles. For both 4T and 3T+F candidates, we require that the back-to-back angle in the transverse plane is consistent with the conservation of transverse momentum. Each full track has an associated momentum, and we define

$$\vec{p}_{123} = \sum_{i=1}^{3} \vec{p}_i$$

and denote the component of this momentum in the plane perpendicular to the K_L^o as $\vec{p}^{\perp}_{123}$. Then

$$\cos\phi_{123,4} = \vec{p}^{\perp}_{123} \cdot \vec{p}^{\perp}_{4} \approx -1$$

and we demand $(1 + \cos\phi_{123,4}) < 0.025$. Furthermore, we compute $p_0'^2$ for all pairs of tracks and take the value closest to zero, which corresponds to assigning pion masses to a particular (+-) pair. We require $p_0'^2 > -.020$ for

the chosen pair, thereby reducing potential contamination due to leptonic decays and beam interactions.

At this point, the analysis for 4T and 3T+F data diverges. The background for the 3T+F candidates is somewhat harder to understand, and consequently we prefer to regard the 3T+F data as a consistency check for the 4T sample. After the aforementioned cuts, the 672 original 4T candidates are reduced to 10. We construct $\vec{p}_{1234}$ and the corresponding direction $\hat{\epsilon}_{1234}$

$$\vec{p}_{1234} = \sum_{i=1}^{4} \vec{p}_i \quad \text{and} \quad \hat{\epsilon}_{1234} = \frac{\vec{p}_{1234}}{|\vec{p}_{1234}|}$$

For signal, $\hat{\epsilon}_K$ and $\hat{\epsilon}_{1234}$ must be colinear:

$$\cos\theta_{1234,K} = \hat{\epsilon}_K \cdot \hat{\epsilon}_{1234} \approx 1$$

We find that the 10 candidates scattered widely on the $\cos\theta_{1234,K}$ plot, with no events remaining in the region $1.0 - \cos\theta_{1234,K} < 2.5\times10^{-6}$ which would contain > 99% of the Monte Carlo data surviving the above cuts.

To confirm our understanding of the origin of the candidates, we generate a sample of $K_L \to \pi^+\pi^-\pi^o$ events wherein the π^o undergoes a subsequent Dalitz decay. We simulate the process using the matrix element given by Joseph.[82] This technique is complicated by the variation of the Dalitz pair matrix element over five orders of magnitude and the sensitivity of the resulting acceptance. After obtaining a reasonable fit to this function, we find 9 events surviving the same cuts made on the data. We conclude that the contamination from $K_{\pi 3}$ decays alone is sufficient to account for the observed candidates, and the distributions appear to be reasonably reproduced.

In addition we have a consistency check in the 4T data using the 3T+F events, for which there are originally 4073 candidates. We impose the same

restrictions as for 4T candidates, with the additional demand that the missing track would not have passed through the magnet if the decay were actually $K_L \to \pi\pi ee$. The momentum of the fourth track is computed assuming the conservation of transverse momentum:

$$|\vec{p}_4| = \frac{|\vec{p}_{123}|}{\sin \theta_{4K}}$$

where θ_{4K} is the angle between the fourth prong and the kaon. For the data, we observe 6 candidates after the above cuts, and from the $K_{\pi 3}$ simultation, we expect to have 4.8. (Without the "back-to-back" cut on $\cos \theta_{123,4}$, we would have 20 candidates and would expect 17 from $K_{\pi 3}$ decays.) Although the statistics are poor, we believe that we would detect real $K_L \to \pi\pi ee$ events if they were present, and also that we understand the behavior of the background. We learn the acceptance by generating $K_L \to \pi\pi ee$ decays using a phase-space distribution only, and this together with the observed distributions allows the computation of the upper limit for this process. We see no events (for the 4T sample at $(1 - \cos \theta_{1234,K}) < 0.25 \times 10^{-6}$) and would expect 2.3 events corresponding to a 90% confidence level. Therefore the number of $\pi\pi ee$ decays is

$$N(\pi\pi ee) \leq -2.3 + 2.3\,\sigma$$

$$\sigma = \left(\sigma^2_{OBS} + \sigma^2_{EXP}\right)^{1/2}$$

and

$$\sigma_{EXP} \simeq \sqrt{2.3}$$

$$\sigma_{OBS} = 1 \text{ (for none observed)}$$

so that

$$N(\pi\pi ee) \leq -2.3 + 4.18 \simeq 1.88 \text{ events}$$

and the branching ratio at 90% C.L. is

$$BR \leq \frac{1.88}{\epsilon_{\pi\pi ee}} \times 3.146 \times 10^{-8}$$

$$\leq 7.2 \times 10^{-6} \quad .$$

This is consistent with the 3T+F data, which has 6 events in the data, and 4.83 events expected from background. In this case, the upper limit would be $\sim 2 \times 10^{-5}$.

This upper limit improves the current experimental value of 3×10^{-5}; however, it is well above the rate expected from γ conversion in the decay $K_L \to \pi\pi\gamma$ as well as the theoretical predictions (of order $10^{-7} - 10^{-9}$) discussed in Section I.

SUMMARY

This experiment has established the following branching ratios:

$\Gamma(K_L^o \rightarrow \pi^+\pi^-\gamma)/\Gamma(K_L^o \rightarrow \text{all}) = (6.2 \pm 2.1) \times 10^{-5}$

$\Gamma(K_L^o \rightarrow \mu^+\mu^-\gamma)/\Gamma(K_L^o \rightarrow \text{all}) \leq 7.81 \times 10^{-6}$ 90% C.L.

$\Gamma(K_L^o \rightarrow \mu^+\mu^-\pi^o)/\Gamma(K_L^o \rightarrow \text{all}) \leq 5.66 \times 10^{-5}$ 90% C.L.

$\Gamma(K_L^o \rightarrow \pi^+\pi^-e^+e^-)/\Gamma(K_L^o \rightarrow \text{all}) \leq 7.2 \times 10^{-6}$ 90% C.L.

$\Gamma(K_L^o \rightarrow \pi^o\pi^\pm e^\mp \nu)/\Gamma(K_L^o \rightarrow \text{all}) \leq 2.2 \times 10^{-3}$ 90% C.L.

REFERENCES

1. H. Fearing, E. Fishbach, J. Smith, "Soft-Photon Theorems and Radiative $K_{\ell 3}$ Decays," Phys. Rev. Letters 24, 189 (1970).
2. M. Doncel, "Comments on Radiative K_{e3} Decays," Phys. Letters 32B, 623 (1970).
3. G. Intemann, "Current Algebra, Vector Dominance, and the Decay $K_L^o \rightarrow \pi^+\pi^-\pi^o\gamma$," Phys. Rev. D 3, 190 (1970).
4. J. Bernstein, G. Feinberg, T. D. Lee, "Possible C, T Noninvariance in the Electromagnetic Interaction," Phys. Rev. 139, B1650 (1965).
5. R. Abrams, A. Carroll, T. Kycia, K. Li, J. Menes, D. Michael, P. Mockett, R. Rubenstein, "Evidence for Direct Emission in the Decay $K^\pm \rightarrow \pi^\pm\pi^o\gamma$," Phys. Rev. Letters 29, 1118 (1972).
6. R. Abrams, A. Carroll, T. Kycia, K. Li, J. Menes, D. Michael, P. Mockett, R. Rubenstein, "Test of CP Noninvariance in the Decay $K^\pm \rightarrow \pi^\pm\pi^o\gamma$," Phys. Rev. Letters 30, 500 (1973).
7. G. Bergun, P. Bertranet, E. Lesquoy, A. Muller, E. Pauli, S. Zylberajch, F. James, L. Montanet, E. Paul, P. Saetre, D. Sendall, "Measurement of the $K_S^o \rightarrow \pi^+\pi^-\gamma$ Decay Rate," Phys. Letters 46B, 481 (1973).
8. L. B. Okun and C. Rubbia, Proceedings of the Heidelberg International Conference on Elementary Particles, 1967; p. 317.
9. A. Dolgov and L. Ponomarev, "On Possible Effects of the Violation of CP invariance in the Radiative Decays of Neutral K Mesons," Soviet Journal of Nuclear Physics 4, 262 (1967).
10. G. Costa and P. Kabir, "Possible CP Noninvariant Effects in $\pi\pi\gamma$ Decay of Neutral Kaons," Nuovo Cimento 51A, 6264 (1967).

11. L. Sehgal and L. Wolfenstein, "CP Violating Interference Effects in Radiative K^0 Decays," Phys. Rev. 162, 1362 (1967).

12. D. Beder, "Suggested Experimental Test of CP Noninvariance in $K^0 \to \pi^+\pi^-\gamma$," Nucl. Phys. B47, 286 (1972).

13. C. S. Lai, B. L. Young, "Calculation of the Decay Rate of $K_2^0 \to \pi^+\pi^-\gamma$," Nuovo Cimento 52A, 7303 (1967).

14. H. Chew, "Final State Interaction and CP Invariance in Radiative $K_{\pi 2}$ Decay," Nuovo Cimento 26, 4941 (1962).

15. S. V. Pepper and Y. Ueda, "Decay Mode $K \to 2\pi+\gamma$," Nuovo Cimento 33, 4894 (1964).

16. S. Oneda, Y. S. Kim, D. Korff, "SU(3) Symmetry and the Nonleptonic K-Meson Processes," Phys. Rev. 136, B1064 (1964).

17. D. Cline, "Possible Test of CP Violation and the $|\Delta T| = 1/2$ Rule for Radiative K-Meson Decays," Nuovo Cimento 36, 1055 (1965).

18. R. C. Thatcher, "An Upper Unit in the Decay Rate of $K_L^0 \to \pi^+\pi^-\gamma$," University of Illinois Thesis, COO-1195-113. See also Ref. 37.

19. All branching ratios quoted herein are from the "Review of Particle Properties," Rev. Mod. Phys. 45 (1973).

20. R. Rockmore, "Pion-Pole Mechanism and the Application of the Veneziano Model to $K_2^0 \to \pi^+\pi^-\gamma$ Decay," Phys. Rev. D 1, 226 (1970).

21. S. Barshay, "A Suggestion Concerning the Present Anomaly in Rate $(K_L \to \mu^+\mu^-)$/Rate $(K_L \to 2\gamma)$," Phys. Letters 36B, 571 (1971).

22. M. Moshe and P. Singer, "Weak Radiative Decays of K Mesons," Phys. Rev. D 6, 1379 (1972).

23. M. Moshe and P. Singer, "Nonleptonic Hamiltonian, SU(3) Breaking, and the $K_2^0 \to \gamma\gamma$ Decay," Phys. Rev. Letters 27, 1685 (1971).

24. M. Moshe and P. Singer, "The Direct Decay $K^+ \to \pi^+\pi^0\gamma$ and its Relation to Other Weak Radiative Decays," PRINT 74-1257 (Tel Aviv) (1974).

25. P. Singer, Proceedings of International Conference on Meson Resonances and Related Electromagnetic Phenomena, Bologna, 1971.

26. A. Browman, J. DeWire, B. Gittelman, K. Hanson, E. Loh, R. Lewis, "Radiative Width of the η Meson," Phys. Rev. Letters 32, 1067 (1974).

27. J. Steinberger, "On the Use of Subtraction Fields and the Lifetimes of Some Types of Meson Decay," Phys. Rev. 76, 1180 (1949).

28. R. Rockmore and T. Wong, "$K_2^0 \to \gamma\gamma$ Decay in a Current-Current Quark Model," Phys. Rev. Letters 28, 1736 (1972).

29. R. Rockmore, J. Smith, T. Wong, "$K^\pm \to \pi^\pm\pi^0\gamma$ Decays in a Current-Current Quark Model," Phys. Rev. D 8, 3224 (1973).

30. A. Kamal and R. Rockmore, "$K^+ \to \pi^+\gamma\gamma$ Decay in a Current-Current Quark Model and a Unified Approach to Weak Radiative Kaon Decays," Phys. Rev. D 9, 752 (1974).

31. R. Rockmore and T. F. Wong, "Calculation of $K_2^0 \to \pi^+\pi^-\gamma$ Decay as a Consistency Test of a Current-Current Quark Model," Phys. Rev. D 7, 3425 (1973).

32. G. Donaldson, D. Hitlin, R. Kennelly, J. Kirkby, J. Liu, A. Rothenberg, S. Wojcicki, "Observation of the Decay $K_L^0 \to \pi^+\pi^-\gamma$," Phys. Rev. Letters 33, 554 (1974).

33. H. Stern and M. Gaillard, "Review of the $K_L \to \mu^+\mu^-$ Puzzle," Ann. Phys. 76, 580 (1973).

34. D. Nygren, "Review of K^0 Decays," LBL-2407, Lawrence Berkeley Laboratory (1973).

35. A. Clark, T. Elioff, R. Field, H. Frisch, R. Johnson, L. Kerth, W. Menzel, "Experimental Limits on the Decays $K_L^o \to \mu^+\mu^-$, e^+e^-, and $\mu^\pm e^\mp$," Phys. Rev. Letters 26, 1667 (1971).

36. N. Chang and E. Ma, "Neutral K-Meson Decay into 2π, 2μ, 2γ Channels: A Unitarity Analysis," PRINT 72-2271, City College of New York (1972).

37. R. C. Thatcher, A. Abashian, R. J. Abrams, D. W. Carpenter, R. E. Mishke, B.M.K. Nefkens, J. H. Smith, L. J. Verhey, A. Wattenberg, "Upper Limit on the Decay Rate $K_L^o \to \pi^+\pi^-\gamma$," Phys. Rev. 174, 1674 (1968).

38. B.M.K. Nefkens, A. Abashian, R. J. Abrams, D. W. Carpenter, G. P. Fisher, J. H. Smith, "Search for the Decay $K_L^o \to \pi^-\pi^+\gamma$," Phys. Letters 19, 706 (1966).

39. E. Bellotti, A. Pullia, M. Baldo-Ceolin, E. Calimani, S. Ciampolillo, H. Huzita, F. Mattioli, A. Sconza, "Experimental Investigation of the $K^o \to \pi^+\pi^-\gamma$ Decay," Nuovo Cimento 45, 6685 (1966).

40. M. Anikina, G. Vardenga, M. Zhuravleva, D. Kotlyarevskii, D. Neagu, E. Okonov, G. Takhtamyshev, Wu Tsung-fan, L. Chkhaidze, "Determination of the Relative Probabilities of $K_L^o \to 3\pi$ Decays," Soviet Journal of Nuclear Physics 2, 609 (1966).

41. B. Martin, E. de Rafael, J. Smith, "Neutral Kaon Decays into Lepton Pairs," Phys. Rev. D 2, 179 (1970).

42. M. Gaillard, "Contribution of the $\pi\pi\gamma$ State to the Decay $K_L \to \mu^+\mu^-$," Phys. Letters 35B, 431 (1971).

43. W. Alles, M. Gaillard, J. Pati, "Comment on the $\pi\pi\gamma$ Contribution to the Absorbtive Amplitude for $K_L \to \mu^-\mu^+$," Phys. Rev. D 8, 2299 (1973).

44. W. Carithers, T. Modis, D. Nygren, T. Pun, E. Schwartz, H. Sticker, J. Steinberger, P. Weihammer, J. Christenson, "Observation of the Decay $K_L^o \to \mu^+\mu^-$," Phys. Rev. Letters 30, 1336 (1973).

45. W. Carithers, D. Nygren, H. Gordon, M. Ioffredo, K. Lai, P. Weihammer, "Further Observation of the Decay $K_L^o \to \mu^+\mu^-$," Phys. Rev. Letters 31, 1025 (1973).

46. As quoted in Ref. 34; reported at APS Conference in Washington, D. C. (1973).

47. J. Primak, "Gauge Theories of Weak and Electromagnetic Interactions," Proceedings of Summer Institute on Particle Physics, Vol. II (1973); p. 91.

48. M. Gaillard and B. Lee, "Rare Decay Modes of the K-Mesons in Gauge Theories," NAL-PUB-74/21-THY (1974).

49. M. Longo, "The Importance of a Measurement of the Decay $K^o \to \mu^+\mu^-\gamma$," PRINT UM-HE-72-19 (1972).

50. T. Miyazaki, "Meson $\to \gamma\ell\bar{\ell}$ Decay as a Test of the $K_L \to \mu\bar{\mu}$ Puzzle," Nuovo Cimento Letters 3, 293 (1972).

51. L. Sehgel, "Structure Effects in the Decays $K_{L,S} \to \gamma$ + Dalitz Pair," Phys. Rev. D 7, 3303 (1973).

52. S. Singh, "CP Nonconservation and $K \to \ell\bar{\ell}\gamma$ Decays," Phys. Rev. D 6, 2646 (1972).

53. W. Alles and J. Pati, "Tests for a Possible Class of CP Invariant Solutions to the $K_L \to \mu\bar{\mu}$ Problem," Nuovo Cimento 10A, 325 (1972).

54. O. W. Greenberg and G. Yodh, "Diffractive Lepton Scattering and Constant $\sigma(e^+e^- \to \text{Hadrons})$: A New Regime in Lepton Physics," Phys. Rev. Letters 32, 1473 (1974).

55. A. Pais and S. Treiman, "Study of the Decays $K \to \ell\bar{\ell}$ and $K \to \pi\ell\bar{\ell}$," Phys. Rev. 176, 1974 (1968).

56. S. Singh and L. Wolfenstein, "Possible Effects of Lepton Nonlocality in the Decays $K \to \pi e^+ e^-$ and $K \to \pi\nu\bar{\nu}$," Nucl. Phys. B24, 77 (1972).

57. S. Okubo and M. Bace, "CP Violating Neutral Leptonic Currents and $K^o_{L,S} \to \mu\bar{\mu}$ Decays," Nucl. Phys. B40, 541 (1970).

58. P. Bloch, S. Brehin, G. Bunce, B. Devaux, A. Diamant-Berger, N. Do-Duc, G. Marel, R. Turlay, P. Exterman, J. Fischer, O. Guisan, R. Mermod, L. Rosselet, R. Sachot, "Observation of the $K^+ \to \pi^+ e^+ e^-$ Decay," PRINT 74-1314 (Saclay) (1974).

59. R. Rockmore and A. Kamal, "Some Rare Decay Modes of the K-Meson in a Current-Current Quark Model; I: $K \to \pi\ell^+\ell^-$ Decay," PRINT 74-1084 Alberta (1974).

60. M. Anikina, V. Balashov, B. Bannik, H. Vardenga, M. Zhuravljiova, V. Iljina, J. Lukstinsh, E. Maltsev, V. Moros, E. Okonov, T. Ostanevich, G. Ttentjukova, J. Cherepanov, S. Khorozov, "A Search for the $K^o_L \to \pi^+\pi^- e^+ e^-$ Decay by Means of the Arrangement SKM-100 with a 1 m Streamer Chamber," PRINT 72-3826 DUBNA (1972).

61. G. Evans, J. Muir, K. Peach, I. Budagov, H. Hopkins, W. Krenz, F. Nezrick, R. Worthington, "Observation of the Radiative Electronic Decay Mode of the Long-Lived Neutral K Meson," Physics Letters 35B, 351 (1971).

62. L. Kondratyuk, L. Panomarev, V. Zakharov, "The Decay $K^o_2 \to \pi^+\pi^- e^+ e^-$ and the Radius of $K^o_2 - K^o_1$ Electromagnetic Transition," Phys. Letters 27B, 655 (1968).

63. V. Lyuboshitz, "Incoherent $K^o_L \to K^o_S$ Regeneration on Atomic Electrons at High Energies, and the Electric Radius of the K^o Meson," ZhETF Pis. Red. 18, 432 (1973).

64. D. Majumador and J. Smith, "Current Algebra, Field-Current Identity, The $K^o_2 K^o_1$ Electromagnetic Transition, and the Decays $K^o \to \pi\pi e^+ e^-$," Phys. Rev. 187, 2039 (1969).

65. A. Pais and S. Treiman, "Pion Phase-Shift Information from $K_{\ell 4}$ Decays," Phys. Rev. 168, 1858 (1968).

66. P. Basile, S. Brehin, A. Diamant-Berger, P. Kunz, M. Lemoine, R. Turlay, A. Zylbersztejn and M. Bourquin, J. Boymund, P. Exterman, J. Marasco, R. Mermod, P. Piroue, H. Suter, "Determination of the Low-Energy $\pi-\pi$ Phase Shifts and Form Factors in K^+_{e4} Decay," Phys. Letters 36B, 619 (1971).

67. R. Ely, G. Gidal, V. Hagopian, G. Kalmus, K. Billing, F. Bullock, M. Esten, M. Govan, C. Henderson, W. Knight, F. Stannard, O. Treutler, U. Camarini, D. Cline, W. Fry, H. Haggarty, R. March, W. Singleton, "Study of K_{e4} Decays," Phys. Rev. 180, 1319 (1969).

68. W. Schweinberger, D. Bertrand, M. Czejthey-Barth, P. Van Binst, W. Knight, J. Lemonne, C. Esueld, F. Bobisut, M. Mattioli, and G. Miari, "An Experimental Study of the Decay Rate, Form Factors and $\pi-\pi$ Phase Shift in K^+_{e4} Decay," Phys. Letters 36B, 246 (1971).

69. F. Berends, A. Donnachie, G. Oades, "A Note on the K_{e4} and $K_{\mu 4}$ Decay Rates," Phys. Letters 26B, 109 (1967).

70. M. Bace and S. Okubo, "Comments on Some Four-Body K^o_L Decays," Phys. Letters 38B, 429 (1972).

71. S. Weinberg, "Current-Commutator Calculations of the $K_{\ell 4}$ Form Factors," Phys. Rev. Letters 17, 336 (1966).

72. W. Carithers, C. Lam, P. Muhlmann, B. Wormington, A. Carroll, I. Chiang, T. Kycia, K. Li, P. Mazur, R. Ruberstein, "AGS Proposal No. 631" (1973).

73. R. Piccioni, "Charge Asymmetry in $K_L^o \to \pi\mu\nu$," Report No. SLAC-155, Stanford Linear Accelerator Center (1972).

74. R. Messner, University of Colorado Thesis (1974).

75. R. Piccioni, G. Donaldson, D. Fryberger, D. Hitlin, J. Liu, B. Meyer, A. Rothenberg, M. Schwartz, D. Uggla, and S. Wojcicki, "Measurement of the Charge Asymmetry in the Decay $K_L^o \to \pi^{\pm}\mu^{\mp}\nu$," Phys. Rev. D 9, 2939 (1974).

76. R. Coombes, D. Fryberger, D. Hitlin, R. Piccioni, D. Porat, "A Data Acquisition System for a Large Wire Chamber Spectrometer," Nucl. Instr. Methods 98, 317 (1972).

77. R. Messner, A. Franklin, R. Morse, U. Nauenberg, D. Dorfan, D. Hitlin, J. Liu, R. Piccioni, "Experimental Determination of the $K_L^o \to \pi^+\pi^-\pi^o$ Decay Matrix Element," Paper 882 submitted to XVI International Conference on High Energy Physics, Chicago, 1972.

78. G. Donaldson, D. Fryberger, D. Hitlin, J. Liu, B. Meyer, R. Piccioni, A. Rothenberg, D. Uggla, S. Wojcicki, D. Dorfan, "Measurement of the Form Factors in the Decay $K_L^o \to \pi\mu\nu$," Phys. Rev. D 9, 2960(1974).

79. B. Rossi, High Energy Particles (Prentice Hall, Englewood Cliff, New Jersey, 1952).

80. D. Sober, R. Haddock, B. Nefkens, B. Schrock, "An Experimental Study of Photon-Initiated Showers in Lead Between 150 and 450 MeV," Nucl. Instr. Methods 109, 29 (1973).

81. V. V. Barmin, G. Davidenko, V. Demidov, A. Dolgolenko, V. Matveev, A. Meshkovskii, G. Mirosidi, T. Chistyakova, I. Chuvilo, V. Shebanov, "Search for a Neutral Vector Meson in K_L Decays," Soviet Journal of Nuclear Physics 15, No. 6, 636 (1972).

82. D. Joseph, "Electron Pair Creation in π^-+p Capture Reactions from Rest," Nuovo Cimento XVI, No. 6, 997 (1960).